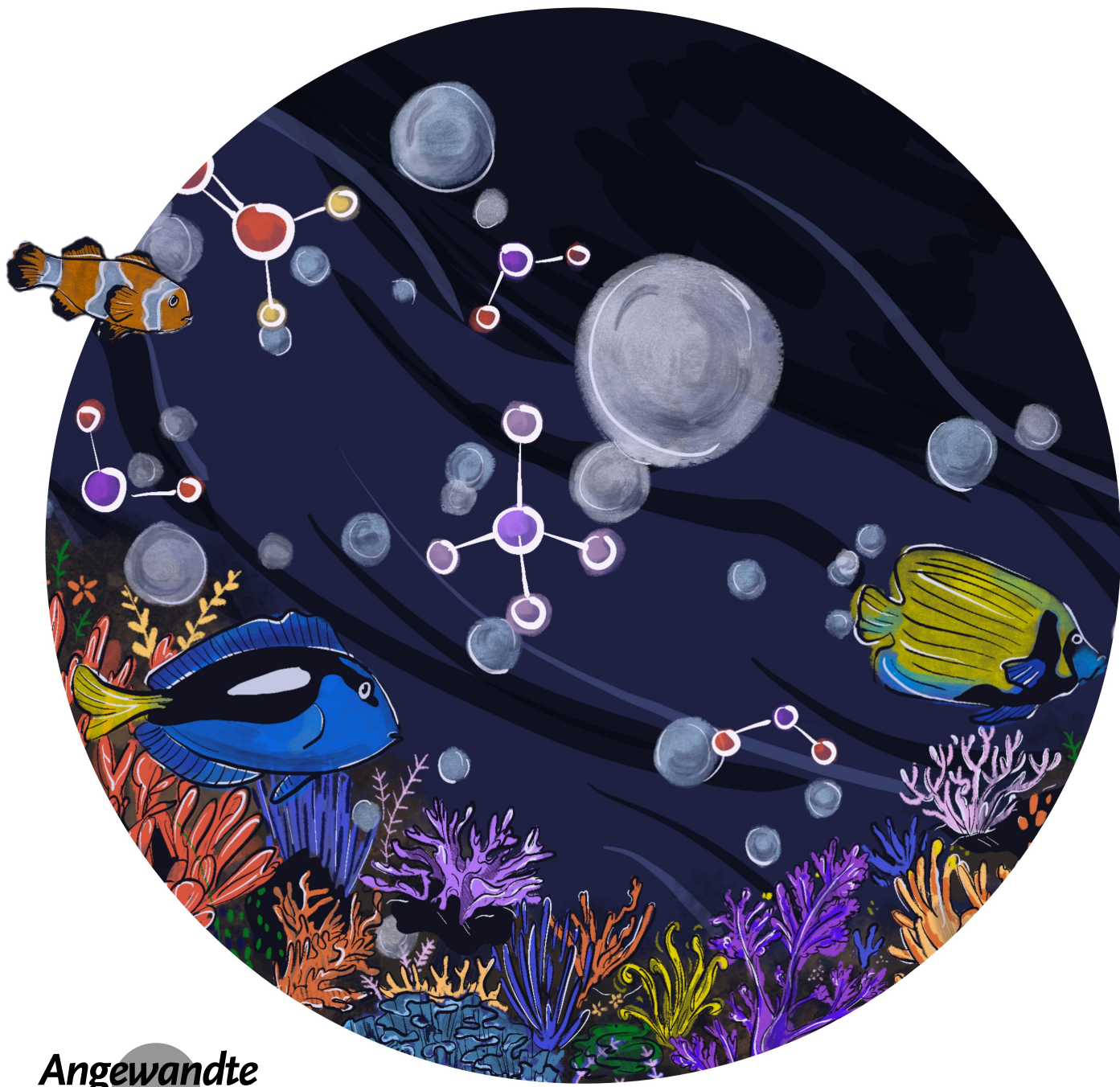


Multiphasic Continuous-Flow Reactors for Handling Gaseous Reagents in Organic Synthesis: Enhancing Efficiency and Safety in Chemical Processes

Annechien A. H. Laporte, Tom M. Masson, Stefan D. A. Zondag, and Timothy Noël*



Abstract: The use of reactive gaseous reagents for the production of active pharmaceutical ingredients (APIs) remains a scientific challenge due to safety and efficiency limitations. The implementation of continuous-flow reactors has resulted in rapid development of gas-handling technology because of several advantages such as increased interfacial area, improved mass- and heat transfer, and seamless scale-up. This technology enables shorter and more atom-economic synthesis routes for the production of pharmaceutical compounds. Herein, we provide an overview of literature from 2016 onwards in the development of gas-handling continuous-flow technology as well as the use of gases in functionalization of APIs.

1. Introduction

The production of active pharmaceutical ingredients (APIs) and advanced intermediates for the preparation of fine chemicals has traditionally relied on batch processing, due to a great variety and availability in reactor types.^[1,2] However, one of the limitations of these batch reactors is the performance of multiphasic reactions in a safe and efficient manner.^[1] Reactions with gaseous substrates are typically complicated reactions to perform in conventional batch equipment due to low interfacial areas, slow diffusion of the gas into the reaction mixture, and safety issues concerning the headspace.^[3,4] In batch equipment, high concentrations of gases are often present in the headspace, where mixing with reaction fumes can result in safety hazards.^[3] Reactions with gases are therefore restricted in terms of equipment, pressure ranges, temperature ranges, and low stoichiometries of the reactive gaseous compounds.^[3,5,6]

However, the most direct, atom-efficient, and therefore often the most sustainable synthetic route frequently requires the use of highly reactive, low-weight, yet toxic gases.^[7] Despite these advantages, they are often banned from laboratories due to safety reasons. Hence, longer manufacturing routes containing easier-to-handle chemicals are frequently chosen instead. The scale-up of the reactions towards API synthesis suffers from this, because these synthetic routes require more labor and result in more waste generation.^[7–9] The development of safe and efficient technologies to handle reactive and low-molecular weight gases is therefore in high demand.^[10]

Previous research has shown that continuous-flow chemistry can play a key role in the safe and effective use of gases in the pharmaceutical industry (Figure 1).^[2,11] In the scope of this review, continuous-flow chemistry is generally a broad term to describe the continuous performance of a reaction within narrow channels (10^2 to $10^3 \mu\text{m}$ range) of micro- or mesofluidic reactors, unless stated otherwise.^[12] These small dimensions allow for several inherent benefits.

[*] A. A. H. Laporte, T. M. Masson, S. D. A. Zondag, T. Noël
Flow Chemistry Group, van't Hoff Institute for Molecular Sciences (HIMS), Universiteit van Amsterdam (UvA)
Science Park 904, 1098 XH, Amsterdam (The Netherlands)
E-mail: t.noel@uva.nl

© 2023 The Authors. Angewandte Chemie International Edition published by Wiley-VCH GmbH. This is an open access article under the terms of the Creative Commons Attribution License, which permits use, distribution and reproduction in any medium, provided the original work is properly cited.

First, the total inventory of hazardous material in a continuous-flow reactor is relatively low leading to an inherent improved safety, which allows the use of hazardous gases like oxygen.^[3,13,14] Moreover, the improved heat transfer in microreactors decreases the potential for hotspot formation and headspace issues —often observed in traditional batch setups— are prevented.^[3] Finally, the increased interfacial area allows efficient mass transfer within the reaction mixtures, which boosts reaction kinetics.^[5,6,10] This larger interfacial area also translates to an enhanced irradiation of the reaction mixture improving the photon availability for photochemical multiphasic reactions.^[15,16]

Over the last years, pharmaceutical companies have invested in continuous-flow technology for synthesis as well as drug discovery to address the need for new, robust, selective, and scalable processes.^[18–21] Flow-chemistry methodology has been developed for reactions at extreme temperatures, hazardous reagents and gases, as well as photo- and electrochemical reactions due to more efficient energy transfer.^[19] Recent advances allow for the multistep preparation of complex molecules (such as APIs) in a telescoped manner, although this remains a challenge.^[7,22–24] Additionally, the scale-up of continuous-flow microreactors from laboratory to industrial scale is promising through numbering-up strategies and would range for API development from g h^{-1} to kg h^{-1} (Figure 2).^[18,25–27]

A review on the use of gases in continuous-flow reactors was published in 2016 by Baxendale and co-workers.^[5] Since this research field is rapidly developing, this review attempts to provide an overview of recent publications on new technologies to handle gases and improved synthetic routes

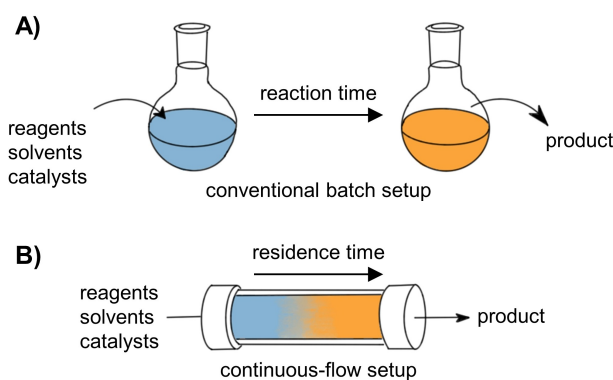


Figure 1. Difference between A) batch and B) continuous-flow reactions.^[17]

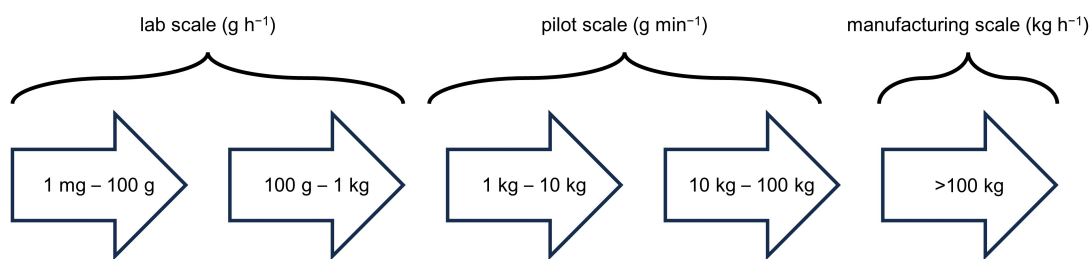


Figure 2. Required quantities of APIs in the various phases of process development.^[18]

to produce high value molecules using gaseous reagents in combination with solid and liquid reagents in flow.

2. Continuous-flow setups for handling gas–liquid reactions

2.1. Chip- and coil-based reactors

In common laboratory continuous-flow experiments, biphasic gas–liquid reactions are often performed in micro/milli-reactors that can be either chip- or coil-based reactor units (Figure 3).^[4] These reactors are the most widely accessible and have a large variety in applications.^[28] Chip-based reactor units offer improved heat transfer characteristics compared to other reactor designs, because of their

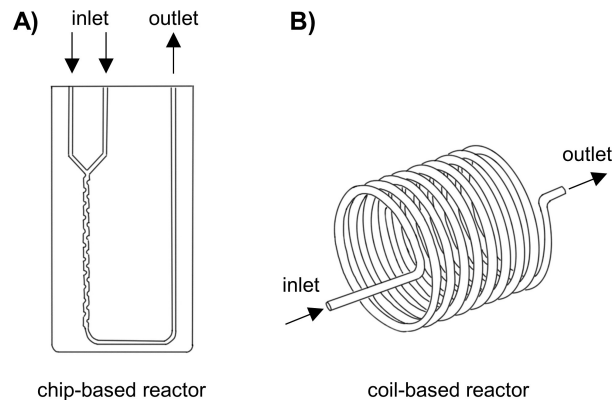


Figure 3. Common reactor types to perform biphasic flow reactions. A) An example of a chip-based reactor from Little Things Factory. B) A coil-based reactor.



Annechien Laporte received both her BSc and MSc degrees in Molecular Chemistry at the University of Amsterdam and Vrije Universiteit. Previously, she worked on biphasic dye-sensitized photoelectrochemical cells for alcohol oxidation in the Homogeneous Catalysis group of the University of Amsterdam. During her MSc she worked on the synthesis, characterization, and performance evaluation of heterogeneous catalysts for tandem electrocatalytic CO_2 reduction at Uppsala University in the Synthetic Molecular Chemistry group.



Tom Masson received both his MSc and chemical engineering degrees from the National Engineer school of Mulhouse. Later, he worked for Servier laboratories in Budapest on the synthesis of protein inhibitors as anti-cancer agents. For his MSc thesis Tom conducted work at Idorsia pharmaceuticals in Basel on the synthesis of new scaffolds in cancer treatment. At Idorsia pharmaceuticals, he investigated the implementation of new methods of synthesis. Currently, he is a Ph.D. student at the University of Amsterdam working on photocatalysis in flow.



Stefan Zondag received both his BSc in Chemical Engineering and Chemistry and his MSc in Chemical and Process Technology at Eindhoven University of Technology. During his Master he conducted research at Queen's University in Belfast, focused on hydrodynamic and acoustic cavitation technology. He finished his Master thesis on application and simulation of ultrasonic devices at the group of Micro Flow Chemistry in Eindhoven. Currently, he is a Ph.D. candidate at the University of Amsterdam, working on modelling of photochemical reactors.



Timothy Noël is Full Professor and Chair of Flow Chemistry at the University of Amsterdam, where he focuses on the synergy between synthetic organic chemistry and technology. He has received several awards, including the DECHEMA prize (2017), Hoogewerff Jongerprijs (2019), IUPAC-ThalesNano prize (2020), KNCV Gold Medal (2021), ACS Sustainable Chemistry & Engineering Lectureship Award (2022), and ChemSocRev Pioneering Investigator Lectureship (2023). He is Editor-in-Chief of the Journal of Flow Chemistry, president of the Flow Chemistry Society, and co-organizer of #RSCPoster.

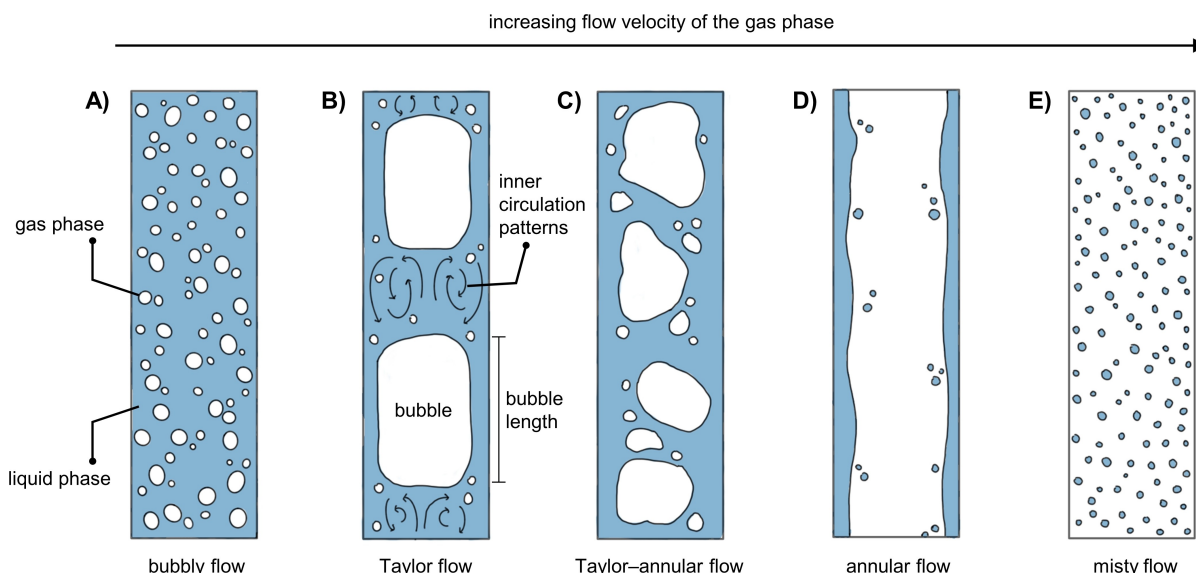


Figure 4. Main flow regimes observed in biphasic flow reactions with increasing flow velocity of the gas phase from left to right: A) bubbly flow. B) Taylor flow. C) Taylor-annular flow. D) annular flow. E) misty flow.^[5]

extremely high surface/volume ratio and the potential use of materials with high thermal conductivity (e.g., silicon carbide).^[4]

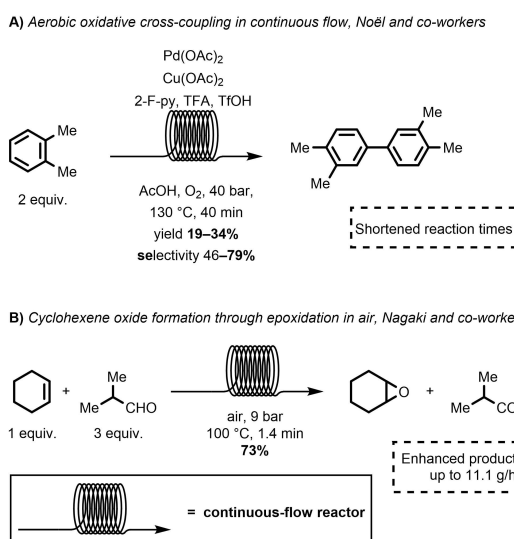
Coil-based reactor units are the most widely used alternative to the chip-based ones, as they can be made from commercially available tubing.^[4,28] This tubing is generally cheap and often consists of inert fluoropolymers or stainless-steel capillaries. Coil-based reactors are frequently structured as helically coiled tubes, which has several advantages: forming a helix from the coil makes the reactor significantly more compact, reducing the physical space occupied by the unit. Moreover, the internal-flow heat transfer coefficient is higher of a helically coiled tube.^[29,30] Using these helically coiled tubes, Noël and co-workers demonstrated a numbering-up strategy for biphasic gas–liquid reactions in flow.^[31] Numbering up is a practical way to scale up a chemical reaction without increasing the pressure drop in the system. The authors managed to keep a constant flow distribution that resulted in a comparable yield output between a single reactor and eight reactors in parallel.^[31,32]

2.1.1. Introduction to flow regimes

The behavior of gases and liquids is very different in microchannels compared to tubes with large diameters or batch reactors. The combination of gas and liquid phase in microchannels can result in various flow patterns, which are influenced by the channel properties of the reactor, the flow rates of the two phases, and the respective viscosities (Figure 4).^[4,5]

Most commonly, Taylor flow is observed, in which bubbles of gas are separated by slugs of liquid (Figure 4B).^[33] This flow regime occurs when the gas and liquid phase have similar, low flow velocities ($< 1.0 \text{ ms}^{-1}$).^[34] A significant advantage of using Taylor flow is its improved

mass transfer performance.^[35] This is first of all governed by the interfacial area, which is in turn determined by the length of the slug and the thickness of the liquid layer between the gas bubble and the inner wall. The slug length is influenced by the flow rates of the two phases. Second of all, the inner circulation patterns observed in Taylor flow play a major role in the mass transfer efficiency.^[35] The Noël group took advantage of these increased mixing properties in Taylor flow to significantly reduce the reaction time of cross-coupling reactions in microreactors (Scheme 1A).^[36] High temperatures (130 °C) and pressures (40 bar) were employed to demonstrate the production of 3,4,3',4'-tetramethylbiphenyl through aerobic oxidative coupling.



Scheme 1. A) Aerobic oxidative cross-coupling reaction in continuous flow.^[36] B) Epoxidation of cyclohexene in air with isobutyraldehyde to form cyclohexene oxide.^[37]

These shortened reaction times were attributed to the improved mass transfer between the gas and liquid phase, as well as the aforementioned recirculating patterns and the use of pure oxygen to re-oxidize the palladium catalyst.

Using a similar approach, Nagaki and co-workers presented the use of biphasic flow to increase yields and decrease reaction times of previously described batch transformations.^[37] They performed the continuous-flow synthesis of cyclohexene oxide in a reactor consisting of stainless-steel tubing. In their flow setup, the highest yield (84 %) was obtained after 1.4 min at 100 °C (Scheme 1B). These were improved results compared to those obtained through a traditional batch setup, in which the highest yield (75 %) was achieved after ca. 260 min reaction time at 80 °C. This improvement is the result of various benefits, such as the ability to use increased pressures and temperatures in continuous-flow systems as well as the enhanced interfacial area.

Taylor flow is not the only flow pattern to be observed; by increasing the flow rate and concentration of one phase compared to the other, various (transitional) regimes are formed.^[4,33] Understanding these flow regimes is important, as they have different interfacial areas, different mass transfer properties, as well as different residence times in the reactor. These parameters in turn influence the overall reaction rate and the conversion/yield.^[4] Increasing the flow rate of the liquid results in bubbly flow, which is characterized by spherical or distorted gas bubbles which are smaller than or equal to the channel diameter (Figure 4A).^[38–40] In microchannels, the bubbles need to be extremely small to be much smaller than the inner diameter of the channel, making it very unlikely that bubbly flow is observed (Figure 4A and Figure 4E). This is different from Taylor flow, in which the elongated gas bubbles are longer than the inner diameter of the channel.^[4,39] Taylor–annular flow is observed when the velocity of the gas is increased compared to Taylor flow, and gas bubbles start to merge (Figure 4C).^[38,39] When the velocity of the gas is increased even further, annular flow is observed (Figure 4D).^[4,5] The gas stream occupies the core of the channel, pushing the liquid phase against the boundary walls of the microchannels.^[38] This results in a very thin liquid layer, leading to a high interfacial contact area and a short diffusion length, as well as relatively large availability of the gaseous reagent.^[4,41] However, ideal annular flow is often very difficult to achieve since droplets can be dislodged from

the liquid film due to the force of the gas phase.^[42] The occurrence of these dispersed droplets can lead to a deviation from annular flow, and is commonly called misty flow (Figure 4E).^[42]

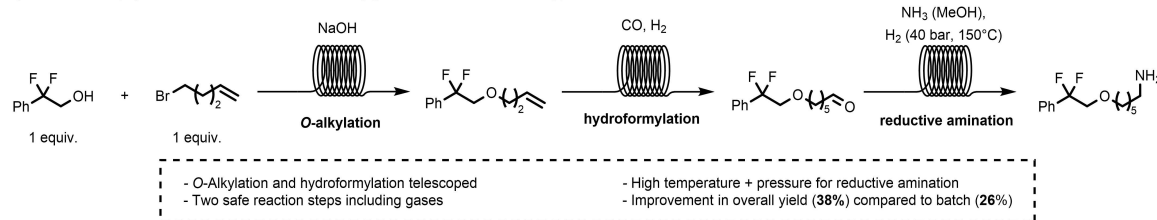
2.1.2. Handling of hazardous gases

Because of the inherent mass transfer advantages of continuous-flow reactors, multiple challenging steps can be sequentially performed, which is called telescoping. For example, Kappe, Hone, and co-workers demonstrated the telescoped synthesis of the lipophilic amine tail of abediterol (Scheme 2).^[43] The key hydroformylation step safely combines toxic carbon monoxide and explosive hydrogen at elevated temperature and high pressure. Because of the continuous-flow synthesis approach, three steps could be performed without isolating or handling the hazardous intermediates of the reaction.

This leads to another major advantage of small channels in continuous-flow reactors, which is that they allow for the usage of gases which are generally considered too hazardous or toxic under conventional batch conditions.^[44,45] This is due to the fact that the operating volume of the reactors are relatively small, ensuring that only a small amount of material is present at any given time. Moreover, no headspace issues are observed in microreactors, and through the use of mass flow controllers the dosage of hazardous gases can be controlled precisely.^[4,44] One example of this is the use of ethylene for the gas–liquid palladium-catalyzed Catellani reaction in continuous flow by Della Ca', Noël, and co-workers (Scheme 3).^[46] According to the authors, the precise control over the stoichiometry of the gaseous reagents played a major role in steering the selectivity to the desired sterically hindered *ortho*-disubstituted styrenes and vinyl arenes.

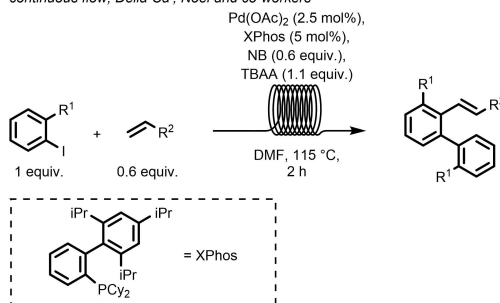
Another example is the use of elemental fluorine, which is a highly toxic, corrosive, and reactive gas. It poses serious safety concerns as exposure can result in severe injury or even have a lethal outcome, which is the reason why the production of fluorinated compounds is often outsourced to specialized laboratories. Nevertheless, Kappe, Dallinger, and co-workers have stated that using F₂ to make fluorinated pharmaceutical compounds would be the most direct route, and therefore atom-economic and cost-efficient.^[47] This is highly desirable, since approximately 50 % of block-

Synthesis of the lipophilic amine tail of an API enabled by gases in continuous-flow, Kappe, Hone and co-workers



Scheme 2. Synthesis of the lipophilic amine tail of an API in continuous flow consisting of subsequent O-alkylation, hydroformylation, and reductive amination using gaseous reagents.^[43]

The use of gaseous ethylene for the gas-liquid palladium-catalyzed Catellani reaction in continuous flow, Delta Ca¹, Noël and co-workers

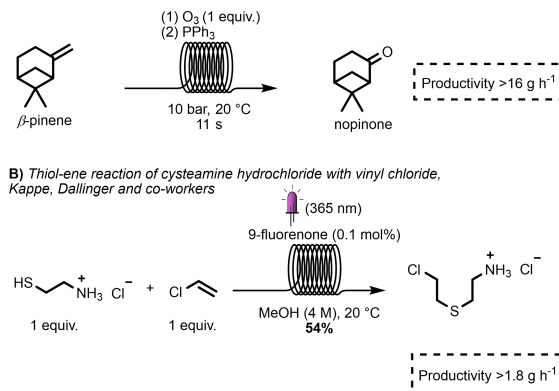


Scheme 3. Use of hazardous ethylene gas for the gas-liquid Pd-catalyzed Catellani reaction in continuous flow.^[46]

buster drugs and 41 % of small pharmaceuticals approved in 2019 by the U.S. Food and Drug Administration contained fluorine atoms because of their enhanced biological properties.^[47,48] In 2022, the Kappe group described a detailed continuous-flow system for the delivery of 10 % fluorine in nitrogen with an overview of suitable reactor components as well as safety precautions.^[47] In a later work, the same group performed the difluoromethylation of a protected amino acid with trifluoromethane gas in continuous-flow to synthesize eflorenthine, an important API (Scheme 4).^[49] The current synthesis strategy consists of an elaborate, multistep synthesis resulting in a processing time of over 23 h and an overall yield of 37–40 %. The newly proposed synthesis route consists of significantly less steps, which improves both the overall yield to 86 % and the processing time to 23.5 min.

Ozonolysis is another valuable reaction that is limited by safety reasons of handling ozone itself as well as its unstable intermediates. In 2021, Roth and co-workers described the design of an ozone dosing line for continuous-flow processing.^[50] They demonstrated the successful synthesis of nopinone from β-pinene, which is a by-product from the paper and pulp industry (Scheme 5A).

A) Ozonolysis of β-pinene to nopinone, Roth and co-workers

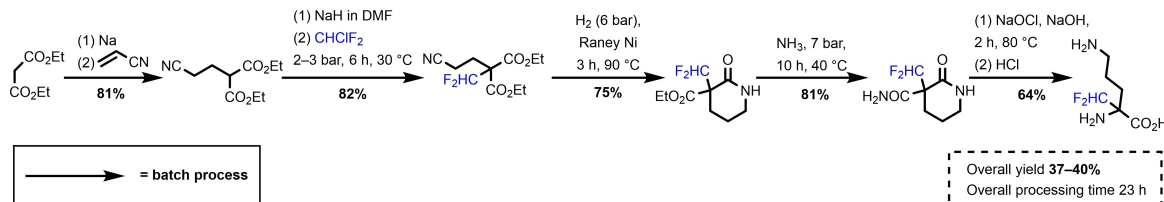


Scheme 5. A) Two-step ozonolysis of β-pinene to nopinone.^[50] B) Thiol-ene reaction of cysteamine hydrochloride with vinyl chloride.^[44]

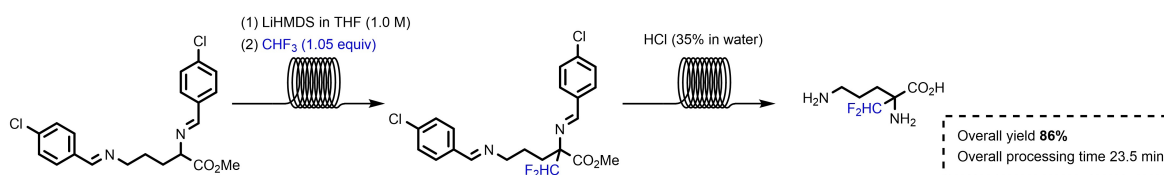
The reaction was safely scaled to >16 g h⁻¹ and a detailed risk assessment was provided. Then, in 2022, the Kappe group made use of the intrinsic safety advantages of microreactors to demonstrate the use of toxic, flammable, and carcinogenic vinyl chloride in the synthesis of thiomorpholine (Scheme 5B).^[44] Moreover, the intermediate that is generated in this pathway is toxic, which emphasizes the need for highly controlled chemistry.

Although these developments improve the atom- and time-efficiency of the reaction pathways, they do not eliminate the need for storage and transport of highly compressed and liquefied gas cylinders. The intrinsic characteristics of microreactors allow for the generation of hazardous reagents from benign precursors *in situ*, which has the advantage of reducing transport, storage, and handling of these compounds.^[7] Moreover, they could be generated on demand in the required volumes, and immediately be transformed into a non-hazardous product upon generation. For example, Noël and co-workers demonstrated the *in situ* generation of the toxic SO₂F₂ gas for the functionalization of

A) Previous industrial synthesis route to eflorenthine starting from diethylmalonate



B) Route proposed by Kappe and co-workers: continuous-flow difluoromethylation using CHF₃



Scheme 4. Comparison between A) the current industrial synthetic route towards the API eflorenthine starting from diethylmalonate, and B) the newly proposed synthetic route in continuous-flow using CHF₃.^[49]

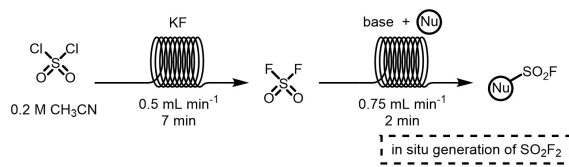
compounds with a $-SO_2F$ group (Scheme 6A).^[51] Their modular flow platform was able to generate SO_2F_2 on demand and safely dose the gaseous reagent, resulting in reduced reaction times and high reactivities for the synthesis of a set of 28 fluorosulfates and sulfamoyl fluorides. The same group also demonstrated the safe use of oxygen gas in a microflow reactor for the oxidation of both unactivated and activated $C(sp^3)-H$ bonds using an inexpensive decatungstate photocatalyst (Scheme 6B).^[52]

Recently, a late-stage photooxidation in continuous flow was demonstrated for the synthesis of *2-epi*-hypatulin B, a highly oxygenated and densely functionalized bicyclic molecule by Christmann and co-workers (Scheme 7A).^[53] The authors developed a synthesis route consisting of 16 steps starting from 2-cyclopentenone. The key synthetic challenge was to develop the bicyclic core in an efficient way, with the oxidative cleavage of an enol ether species at the end in the

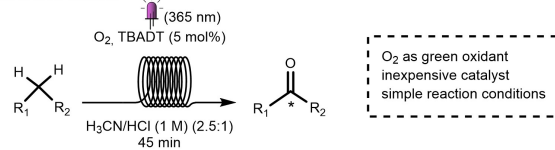
presence of competing alkene functionalities. This reaction was enabled by continuous-flow technology, resulting in larger scales, shorter reaction times, and improved yields. Luisi, Kappe, and co-workers also developed a multistep synthetic route containing a direct α -lithiation step and a hydroxylation through aerobic oxidation step for the continuous-flow preparation of cyclopentylmandelic acid (Scheme 7B).^[54] Their process afforded an overall isolated yield of 50 % after recrystallization, demonstrating the safe use of molecular oxygen for the synthesis of APIs.

One of the most challenging reactions in organic synthesis is the selective functionalization of $C(sp^3)-H$ bonds in gaseous hydrocarbons.^[55,56] This reaction would allow for the conversion of greenhouse gases into chemical feedstocks and is therefore of great value for both the environment as well as the chemical industry, since they are among the most abundant and cheapest feedstocks.^[56] Noël and co-workers demonstrated the use of a photoexcited decatungstate anion ($*[W_{10}O_{32}]^{4-}$) as a hydrogen atom transfer (HAT) photocatalyst that can abstract hydrogen atoms from $C(sp^3)-H$ fragments and form C-centered radicals.^[55,57] To solve the challenge of handling gaseous alkanes in organic solvents, they demonstrated the safe use of microflow reactors at high pressure to force the gaseous alkanes into the liquid phase (Scheme 8A). A related work by Noël and co-workers demonstrated the use of Taylor flow for the photocatalytic carbonylation of light/heavy alkanes to synthesize unsymmetrical ketones (Scheme 8B).^[58] Gaseous light alkanes and toxic carbon monoxide gas are handled as a gas–gas–liquid mixture inside microchannels, to improve mass transfer and create a safe environment for the direct activation of light alkanes.

A) Synthesis of fluorosulfates and sulfamoyl fluorides, Noël and co-workers

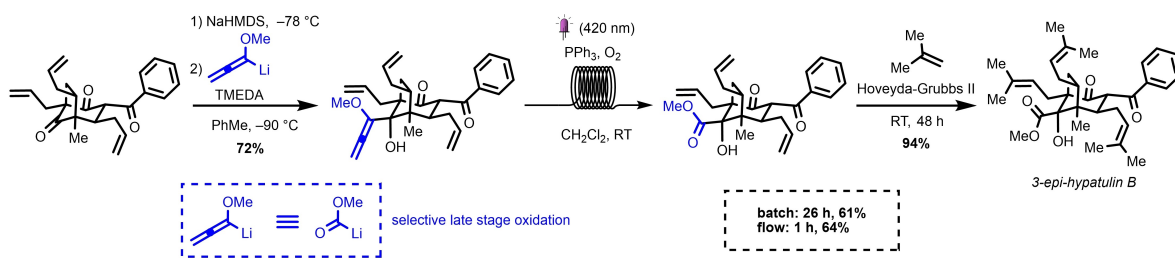


B) Photocatalytic oxidation of $C(sp^3)-H$ bonds using a decatungstate photocatalyst, Noël and co-workers

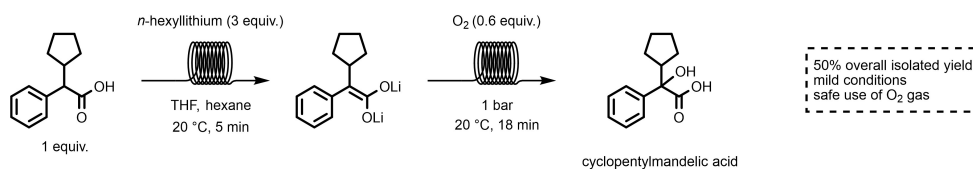


Scheme 6. A) In situ generation of the toxic SO_2F_2 gas for the functionalization of compounds with a $-SO_2F$ group.^[51] B) Photocatalytic oxidation of both activated and unactivated $C(sp^3)-H$ bonds using a decatungstate photocatalyst and O_2 gas.^[52]

A) Synthesis route to *3-epi*-hypatulin B, proposed by Christmann and co-workers

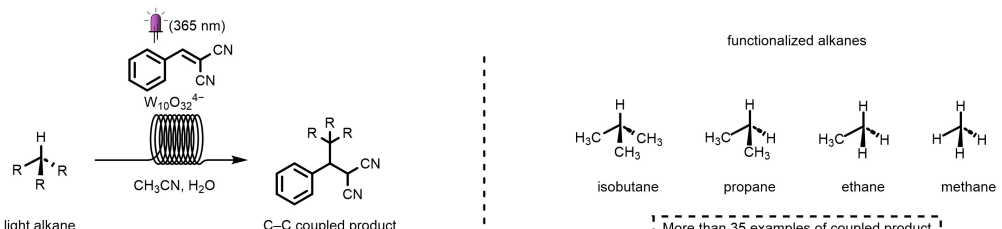


B) Continuous-flow preparation of cyclopentylmandelic acid, Luisi, Kappe and co-workers

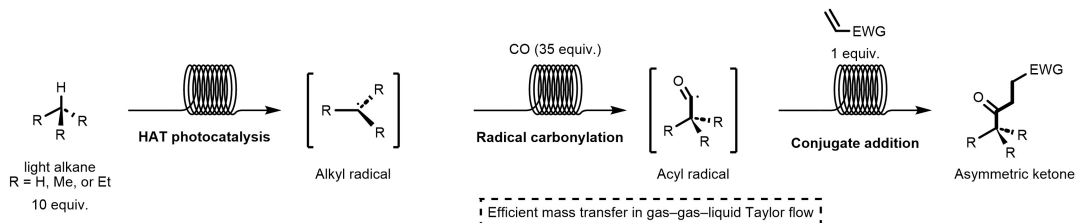


Scheme 7. A) Overall synthesis route for *3-epi*-hypatulin B, including a late-stage selective oxidation step emphasized in blue.^[53] B) Synthesis route towards cyclopentylmandelic acid through an α -lithiation step and a hydroxylation using molecular oxygen.^[54]

A) HAT photocatalysis for the C–C coupling of gaseous alkanes in continuous flow, Noël and co-workers



B) Photocatalytic carbonylation of light/heavy alkanes for the synthesis of asymmetric ketones, Noël and co-workers

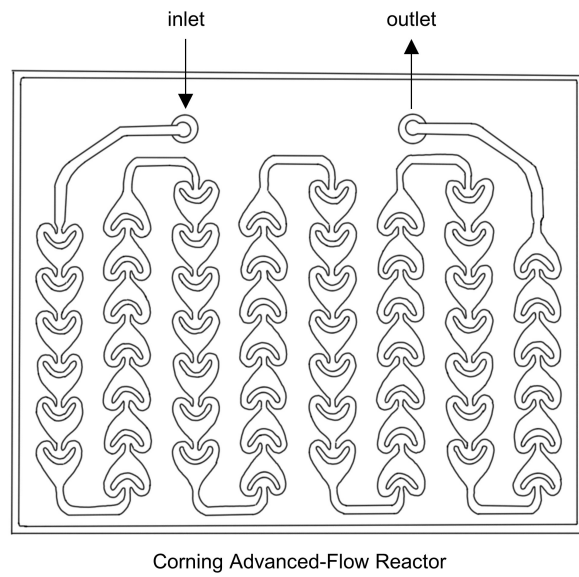


Scheme 8. A) HAT photocatalysis bypasses the need for unselective and low-yielding conversion into alkyl electrophiles to increase the reactivity for eventual C–C coupling.^[55] B) Efficient mass transfer in gas-gas-liquid Taylor flow for the photocatalytic carbonylation of light/heavy alkanes.^[58]

2.1.3. Mass transfer intensification

It is not always straightforward to quantify and compare the interfacial area of the various flow patterns within the channels of a microreactor, as they depend largely on the flow velocity of the two phases. Moreover, the size of the bubbles or slugs observed, as well as the number of bubbles or slugs per time unit are key parameters. With the significant experimental database available in literature for interfacial areas in two-phase flow regimes, recent developments in modelling using interfacial area transport equations are bridging this knowledge-gap. Constitutive models using these equations enable interfacial area predictions from bubbly- to churn-turbulent flow regimes, with extension to annular flow currently being investigated.^[59] Although assumptions must be made, it would be beneficial to have a quantitative description of interfacial areas per flow pattern to support often qualitative statements.

Flow patterns can vary for horizontal and vertical straight pipes. Moreover, flow patterns can be altered through the use of internal mixers to increase the mass transfer.^[60,61] An established microchannel reactor with incorporated static mixers is the Corning Lab Reactor which has been optimized for multiphase mass transfer (Figure 5). In 2017, Monbaliu, Heinrichs, Dreesen, and co-workers described the scalable photocatalytic oxidation of methionine using a Corning Lab Reactor.^[62] They used a biphasic system, consisting of oxygen gas and an aqueous phase. The reactive singlet oxygen species is generated by interaction of oxygen with the excited photosensitizer Rose Bengal in solution. The authors claim that the integrated mixers along the reactor path improved the mass transfer significantly and thereby also the reaction rate, compared to previous work in which a large excess of O₂ was required. A wide variety of design choices for internal mixers and the structure of microchannels are still being explored. For example, Sun and co-workers investigated the optimal



Corning Advanced-Flow Reactor

Figure 5. Corning Lab Reactor: microchip with internal static mixers for improved mass transfer in biphasic reactions.^[64]

structure of microchannels for methanol steam reforming reactions.^[63] They concluded that microchannels in the shape of sinusoidal waves with added dimples showed improved micro-mixing behavior compared to straight channels or channels without dimples. They also suggest that optimizing the shape of microchannels might improve the availability of gas in biphasic reactions.

2.2. Tubular membrane reactors

Tubular membrane reactors have been developed by the Ley group to address the inherent limitations of conventional batch reactors and the most widely used reactor is the

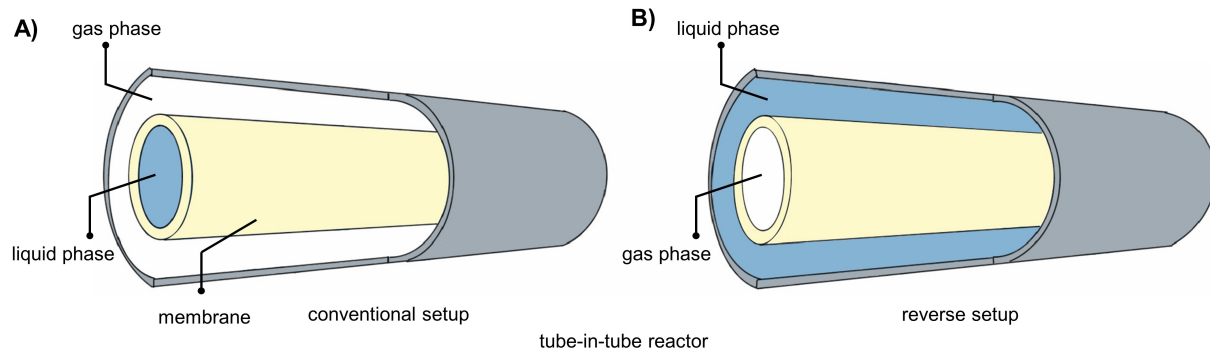


Figure 6. Two configurations in which the tube-in-tube reactor can be set up. A) Conventional mode, with the liquid phase in the inner tube and the gas phase in the outer tube. B) Reverse mode, with the gas phase in the inner tube and the liquid phase in the outer tube.^[74]

tube-in-tube flow reactor.^[65–71] It consists of a smaller gas-permeable tube inside a larger, impermeable tube (Figure 6).^[4,65] The inner tube is made from the generally expensive Teflon AF-2400, which has a relatively high permeability for smaller gas molecules compared to larger, readily condensable gas molecules.^[4,66,72] Moreover, the membrane permeability is higher for reactive gases such as CO, CO₂, and H₂ compared to inert gases such as N₂.^[72] Other gases for which the membrane is permeable are ozone, oxygen, ammonia, ethylene, and diazomethane.^[73] However, nonfluorinated solvents or liquids cannot permeate the membrane due to its chemical resistance, mechanical strength, and microporous and amorphous structure.^[72] This leads to the unique property that only gaseous reagents can pass the membrane to either react with the liquid phase, or to saturate the solvent, and that the outlets are therefore separated for the two phases. The tube-in-tube reactor can be used with either the gas stream in the outer tube and the liquid stream inside, called the conventional configuration (Figure 6A), or with the opposite arrangement, called the reverse configuration (Figure 6B).^[72]

As mentioned before, the interfacial area between the two phases plays a key role in efficient mass transfer, and therefore in improving reaction speed.^[72] Tube-in-tube reactors generally provide exceptionally high interfacial areas as well as mass transfer coefficients compared to other types of reactors (Table 1).^[5,72,75] The values in this table are estimated based on a variety of literature describing differ-

ent reactor types. However, the experiments and setups are not standardized, therefore often difficult to reproduce, and hard to compare. Simulations could play a key role in differentiating between reactor designs. For instance, one quantitative model to analyze the mass transfer in various reactions in tube-and-tube reactors has been developed by Yang and Jensen.^[74] They compared the mass transfer inside the conventional and reverse setup at the same flow rate, demonstrating that the reverse setup provided a higher gas concentration in the liquid phase at the outlet. The authors contributed this result to the fact that flowing the solvent in the outer tube yields a larger cross-sectional area than on the inner tube side. At equal volumetric flow rate, this results in longer gas–liquid contact time and therefore improved mass transfer. Another comparative work was performed by Gobert, Thomassen, and co-workers on the mixing efficiency and residence time distribution in tubular and chip-based milli- and microreactors.^[76]

Apart from the high interfacial area, an additional advantage of microflow reactors is that the stoichiometry of reactive gases in the solution can be precisely controlled using in-line digital imaging.^[65,77] This in-line monitoring allows for high control, which is especially useful for reactions that require high selectivity or make use of extremely hazardous or toxic gases. Ley and co-workers demonstrated the advantages of in-line portable Fourier transform infrared (FTIR) devices as well as nuclear magnetic resonance devices for the accurate dosing of reagents in tube-and-tube reactors for nucleophilic trifluoromethylation in flow.^[73] Using the in-line FTIR instrument, it was first verified that the inner Teflon AF-2400 membrane was permeable to CF₃H. The in-line benchtop nuclear magnetic resonance (NMR) machine recorded ¹⁹F NMR spectra to determine the concentration of the gas dissolved in solution. Moreover, the in-line FTIR was used to screen the optimum reagent concentration for the productivity of the reaction. The process Ley and co-workers described was fully contained and possible dispersion of trifluoromethane was highly controlled and minimized.

A second work that made use of the highly controlled stoichiometry of hazardous gases in tube-in-tube reactions was performed by Wu, Zhang, and co-workers.^[78] They

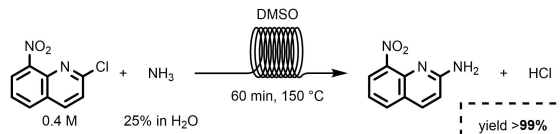
Table 1: Order of magnitude of the interfacial areas for different gas–liquid contactors, where a ($\text{m}^2 \text{ m}^{-3}$) is the interfacial area per volume of the two phases.^[5,72,75]

Type of contactor	a ($\text{m}^2 \text{ m}^{-3}$)
Tube-in-tube	3000–10000
Packed columns, co-current	10–1700
Packed columns, counter-current	10–350
Tube reactors, horizontal and coiled	50–700
Tube reactors, vertical	100–2000
Stirred tank	100–2000
Static mixers	100–1000
Gas-liquid microchannel contactor	3400–18000
Falling film microreactor	20000

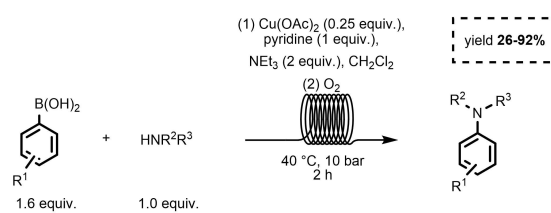
demonstrated the use of aqueous ammonia for the continuous amination of aryl and heteroaryl halides from the hypothesis that NH_3 can diffuse through the AF-2400 tubing at elevated temperatures from readily available and safe aqueous ammonia (Scheme 9A). They state that the tube-in-tube reactor is preferred for such reactions above a biphasic flow regime in microchannels since excess water is detrimental to most organic transformations. The water in the aqueous ammonia mixture is unable to pass the inner membrane at low temperatures and therefore the reaction mixture does not encounter large quantities of water. This improved the yields of various aminations of aryl/heteroaryl halides in a safe and scalable manner.

Using the tube-in-tube technology, Baxendale, and co-workers demonstrated the use of oxygen gas as oxidant in a reversible tube-in-tube reactor for catalytic Chan–Lam C–N coupling reactions for the continuous synthesis of several functionalized aromatic and aliphatic amines (Scheme 9B).^[79] The authors stated that the atom economy of this route was improved over systems utilizing TEMPO (2,2,6,6-tetramethylpiperidinyloxy) and *tert*-butyl peroxybenzoate, and that this setup is safe and scalable. Moreover, the optimization of the reaction conditions demonstrated that the use of sub-stoichiometric amounts of the copper catalyst was more efficient than the stoichiometric amount used in earlier flow studies. Further work by Koolman, Kantor, and co-workers made use of the improved safety of tube-in-tube reactors for the continuous generation and

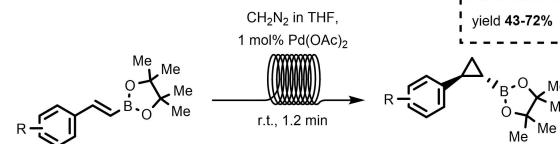
A) Use of aqueous ammonia for continuous amination of aryl and heteroaryl halides,
Wu, Zhang and co-workers



B) Use of oxygen gas for catalytic Chan–Lam coupling, Baxendale and co-workers



C) Pd-catalyzed cyclopropanation reactions for the synthesis of boronic esters,
Koolman, Kantor and co-workers

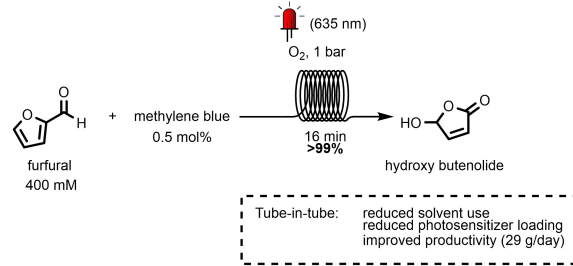


Scheme 9. A) The use of aqueous ammonia in a tube-in-tube reactor system for the continuous amination of aryl and heteroaryl halides, Scheme adapted from Wu, Zhang, and co-workers.^[78] B) Catalytic Chan–Lam coupling by using oxygen gas in continuous flow, scheme adapted from Baxendale and co-workers.^[79] C) Pd-catalyzed cyclopropanation reactions in tube-in-tube reactors for the synthesis of boronic esters, scheme adapted from Koolman, Kantor, and co-workers.^[80]

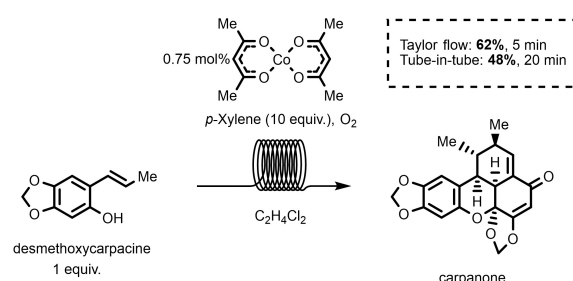
release of diazomethane, which is a highly volatile, explosive, irritating, and severely toxic compound.^[80] They designed an automated flow system to perform palladium-catalyzed cyclopropanation reactions for the synthesis of a small library of cyclopropyl boronic esters, which are of interest as they are readily applicable in cross-coupling reactions, but have limited commercial availability (Scheme 9C).^[80] This automated library synthesis setup could be advantageous for medicinal chemistry, as a variety of closely related structures could provide insight into structure–activity relationships.

It is not always straightforward whether a tube-in-tube system would be beneficial instead of a standard Taylor flow system. In 2022, Feringa and co-workers demonstrated the advantages of using a tube-in-tube reactor over Taylor flow for the continuous-flow photooxidation of furfural (Scheme 10A).^[81] They described the reduced usage of solvent and photosensitizer loading using this setup, as well as improved scalability (29 g/day in quantitative conversion with full selectivity). However, different reactions can benefit from different reactor systems. For example, Felpin and co-workers demonstrated the added value of a Taylor flow compared to a tube-in-tube system through the aerobic dimerization of desmethoxycarpacaine (Scheme 10B).^[82] After various optimization steps of the setups, it was shown that Taylor flow resulted in higher yields (62 % versus 48 %) and shorter reaction times (5 min versus 20 min).^[82] Moreover, the gas loading in tube-in-tube setups is generally low, radial mixing can be insufficient, and the heating characteristics are sub-optimal compared to other continuous-flow reactor types.^[4]

A) Continuous-flow synthesis of hydroxy butenolide from photooxidation of furfural,
Feringa and co-workers



B) Aerobic dimerization of desmethoxycarpacaine to carpanone, Felpin and co-workers



Scheme 10. A) Photooxidation of furfural to hydroxybutenolide.^[81] B) Aerobic dimerization of desmethoxycarpacaine to carpanone.^[82]

2.3. Falling film microreactors

The falling film microreactor (FFMR) is a reactor design based upon the principle that a thin liquid layer allows for a high interfacial contact area and a decreased diffusion length (Figure 7).^[5] It consists of a reaction plate with microchannels (0.3–1.2 mm) embedded in it, above which is a slit that distributes the liquid phase.^[83] This phase flows through microchannels under gravity to form a thin layer (<100 µm), whereas the gas phase can flow co-currently or countercurrently.^[5,84] This design allows for specific gas–liquid interfacial areas of up to 20000 m² m⁻³, which is relatively high compared to other gas–liquid contactors (Table 1).^[75] Although it is conventional that the liquid phase flows parallel to gravity, it is possible to set up FFMRs with inclined reaction plates.^[75] Lokhat and co-workers have demonstrated that the angle of orientation of the reaction plate has a direct influence on the rate of mass transfer, with lower mass transfer coefficients on the liquid phase side at lower plate angles.^[75] Moreover, they observed that the effect of gas flow rate on the liquid-side mass transfer coefficient is negligible at 90° plate angle, but that a significant difference is found between 75° and 60°. This was similarly described by Steinfeldt and Kockmann.^[83] The authors attributed this effect to the influence of the gas flow rate on the hydrodynamics of the liquid phase, inducing a rippling effect and thereby increasing the interfacial area. Another parameter that influences the mass transfer in FFMRs is the thickness of the liquid falling film, because this defines the surface-to-volume ratio and the distance of mass- and heat transfer.^[84] To predict this parameter for various FFMR systems, Tang and co-workers proposed the use of stereo digital microscopy, as this method is cheap, simple, and non-intrusive with adequate accuracy. Moreover, they observed that the film thickness increases with increasing flow rate and increasing viscosity. The thickness of the film has consequences in terms of the residence time distribution: at the walls the effective velocity of the liquid is

zero due to the no-slip condition, whereas the velocity is highest on the outer border.^[85]

An additional benefit of the usage of thin films is the homogeneous irradiation conditions of the reaction mixture, which allows for various photochemical transformations in continuous flow.^[87] In 2018, Oelgemöller and co-workers demonstrated the utility of microfluidic devices for the optimization of chemical processes that include the synthesis of oxygenated products through usage of a commercial FFMR for the photooxygenation of α -terpinene to ascaridole (Scheme 11A).^[87] The large scale photochemical production of this intermediate is hindered by its thermal instability as well as the decreased photochemical efficiency with increased reagent concentration as determined by the Bouguer–Lambert–Beer law. In the FFMR, productivities of 2.5–3.2 mol L⁻¹ h⁻¹ were achieved, which is approximately double the amount achieved in a batch Schlenk flask (0.9–1.2 mol L⁻¹ h⁻¹). The selectivity of the reaction was not affected by reactor design and remained relatively high with 75–80% in both setups. However, in the FFMR the production of large quantities of hazardous oxygenated products was avoided due to the continuous-flow design, improving the safety of this production route. Rehm and co-workers also made use of the improved irradiation properties observed in FFMRs for the continuous-flow photochemically catalyzed synthesis of juglone (Scheme 11B).^[88] The efficient contacting of a gas and liquid phase was combined with high-power light-emitting diode (LED) arrays to produce singlet oxygen in situ for the oxygenation of 1,5-dihydroxynaphthalene to juglone. Although their obtained conversion (97%) and selectivity (99%) were very high, no comparison was made to batch procedures. However, their work described a detailed investigation of the process parameters of photochemical reactions performed in FFMRs: e.g., the irradiation wavelength, LED power, oxygen partial pressure, substrate concentration, and architectural impact of the reactor setup. Moreover, they quantify the quantum efficiency, productivity, and space

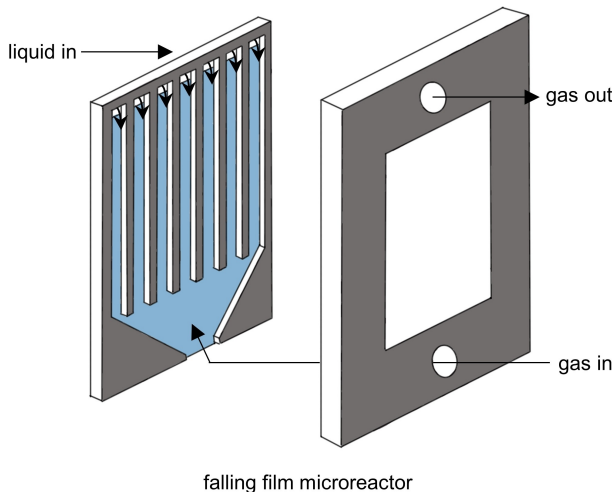
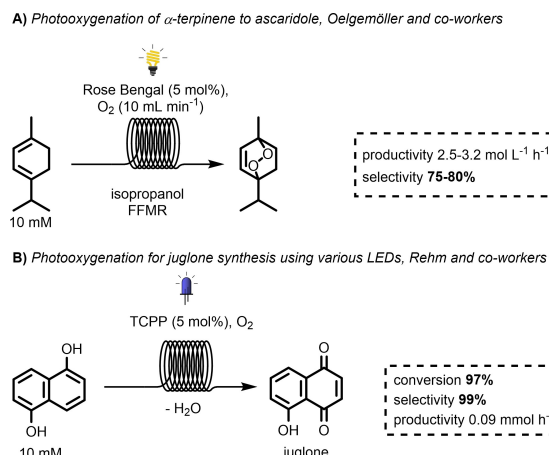


Figure 7. Overview of a falling film microreactor.^[86]



Scheme 11. A) Photooxygenation in a FFMR for the synthesis of ascaridole.^[87] B) Photooxygenation in a FFMR for the synthesis of juglone.^[88]

time yield so that the FFMR can be compared with other reactor types.

FFMRs are also often investigated for usage in wastewater treatment processes as they allow for a larger volume of liquid phase to be treated per time unit. Aziz demonstrated a comparative study of advanced oxidation processes for the removal of pollutants through the systematic use of one setup, for which the FFMR was selected.^[89] It was hypothesized that this reactor could enhance the mass transfer of reactive species from the gas phase to the liquid phase due to the large surface-to-volume ratio. The author states that this would enhance the degradation of chloroacetic acids in aqueous solutions, which are hardly degradable and carcinogenic. A combination of ozone together with photocatalysis and other advanced oxidation processes proved to be most efficient. Another study on the use of FFMRs for the treatment of wastewater was performed by Mao, Che, and co-workers in 2021 on the synthesis of α -FeOOH from wastewater.^[90] The authors used a FFMR with a concentrated oxygen flow to improve the mass transfer between the gas and liquid phase. Because of this, the production efficiency increased 16 times compared to the traditional air method, and the iron recovery rate was >90 %.

In 2021, Mohammed and co-worker described the major challenges and future outlook for FFMRs with emphasis on mass transfer enhancement as well as operational parameters used.^[91] They state that mass transfer is limited from the liquid phase, and that there are still large discrepancies between empirical experiments and the results of hydrodynamic models. Another challenge in this field is the generation of significant volume to enable processing on industrial scale, as conversion is dependent on the flow rate of the liquid phase. The authors stated that the best-case scenario of attainable liquid flow rate without conversion loss would be 3.3 mL min^{-1} in conventional laboratory-sized

reactors. Although there are scaled-up versions of the FFMR (FFMR-large and cylinder) and numbering-up strategies exist, drawbacks in terms of reaction monitoring and process control persist.^[91]

2.4. Rotating continuous-flow reactors

Other reactor designs and flow patterns remain attractive for process intensification purposes. For example, a reactor design called the vortex fluidic device (VFD) was presented to improve mass transfer even further (Figure 8A).^[92] In this reactor, reaction mixtures are rotated at high speeds (0–9000 rpm), so the liquid forms a thin film along the inner walls of the glass tube. According to Raston and co-workers, this setup would yield multiple benefits for biphasic reaction mixtures.^[92,93] First, the thin film would improve the interfacial surface area. Second, the rapid rotation of the inclined tube would lead to more intense mixing to improve mass transfer. Third, a unique environment is created due to shear stress and vibrations to control chemical reactivity.^[94] Finally, the incline of 45° results in unique flow characteristics.^[95] To illustrate these benefits, the Raston group demonstrated the aerobic oxidation of *N*-acetyl-*L*-cysteine in water, in which the mass transfer of oxygen gas into the liquid is rate-limiting (Scheme 12A).^[92] In a batch setup with O_2 in the headspace, 5 % conversion was observed after 1 h. The VFD showed improved results at 7000 rpm using an O_2 stream: 55 % conversion was observed after 5 min. The scale-up of VFDs is not straightforward, but it has been suggested that parallel numbering-up might be effective to reach larger volumes, and scaled, high-throughput VFDs have been demonstrated.^[92,96] A limitation of the VFD might be the operation of reaction mixtures containing highly viscous liquids, which might clog the outlet system.^[97] A rotating reactor making use of the same thin

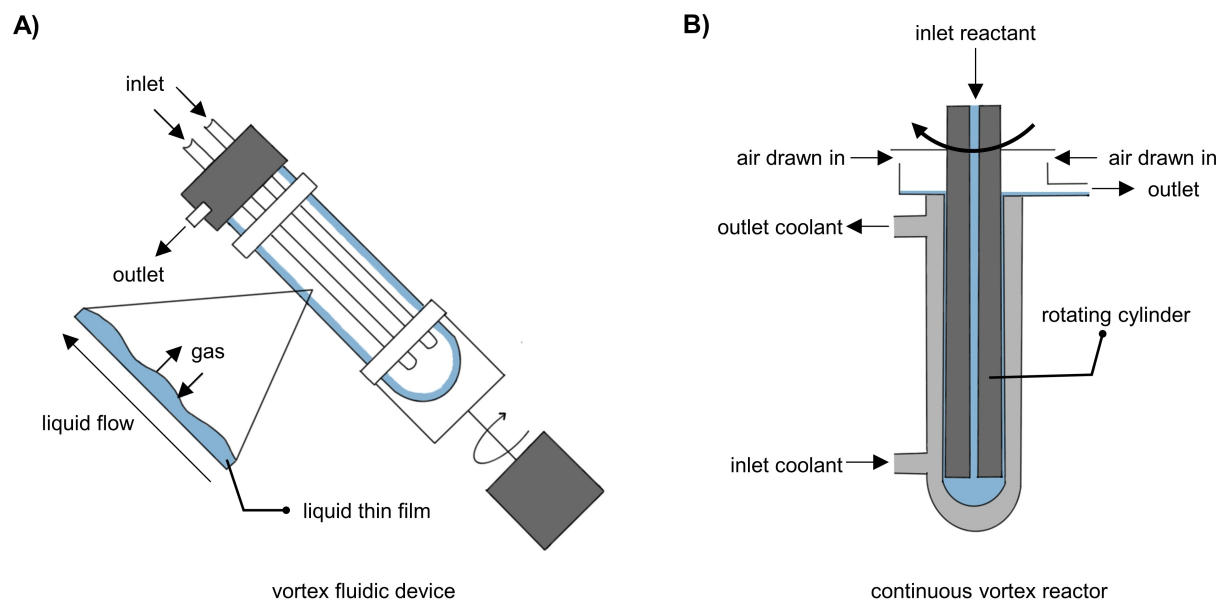
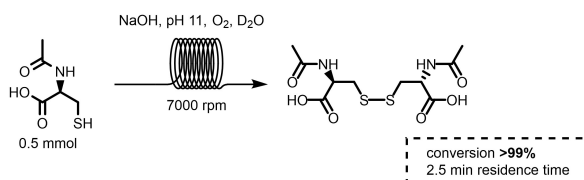
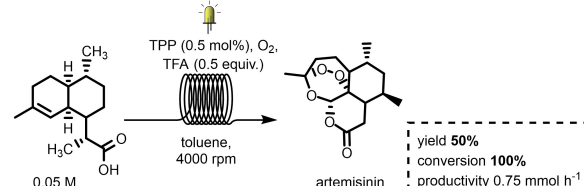


Figure 8. A) A vortex-driven thin film reactor.^[92] B) A continuous vortex reactor.^[100]

A) Aerobic oxidation of N-acetyl-L-cysteine in water in a VFD, Raston, Chalker and co-workers



B) Formation of artemisinin from dihydroartemisinic acid in a continuous vortex reactor, Poliakoff, George and co-workers



Scheme 12. A) Aerobic oxidation of *N*-acetyl-*L*-cysteine in water in a VFD.^[92] B) Formation of artemisinin from dihydroartemisinic acid using singlet oxygen in a continuous vortex reactor.^[100]

film of liquid but based on conventional rotary evaporator equipment has been developed for photochemical transformations.^[98,99]

Another rotating biphasic reactor benefitting from Taylor–Couette flow was developed by George, Poliakoff, and co-workers for several continuous photooxidation reactions using singlet oxygen, such as the formation of artemisinin from dihydroartemisinic acid (Scheme 12B).^[100] This continuous vortex reactor (Figure 8B) rotates slowly compared to the VFD, resulting in micromixing patterns between the gas and liquid phase instead of the thin film formation.^[100] This reactor draws in air from the laboratory, which allows for an elegant alternative to pressurizing with oxygen gas. It was shown that the concentration of oxygen available to react was dependent on the rotation speed of the cylinder, indicating that the optimization of this parameter is key for increasing reaction efficiencies. The authors state that biphasic reactions using hazardous gases can be performed with improved safety in a similar manner to this work, as the concentration of (toxic) gas can be diluted with the available air. Later work by the same group demonstrated the scalability of these reactors for both ultraviolet (UV) and visible photochemistry.^[101] A scaled-up version of the continuous vortex reactor was proposed, which turned at lower rotation speeds in order to keep the level of mixing similar compared to the earlier version. This parameter in turn resulted in an adaptation of the original design: air now had to be fed in using pressurized cylinders in order to saturate the mixture with oxygen. It can therefore be concluded that a tradeoff exists between the scale of the reactor and the need for pressurized cylinders. Various types of continuous vortex reactors have been used for both photochemical and electrochemical transformations.^[96,101,102] The concept of a rotating cylinder is also used for rotor-stator spinning disk reactors, which will be discussed at a later stage.

3. Gas–solid–liquid reactions in continuous flow

There has been increased interest over the past years in new technologies that combine the use of heterogeneous catalysis with continuous-flow chemistry, as several important industrial processes contain gas–solid–liquid phases (e.g., hydrogenations, Fischer–Tropsch, and oxidations).^[103] Moreover, heterogeneous catalysts often allow for ease of separation and as a consequence of this, easier reuse of the catalyst.^[104] However, heterogeneously catalyzed reactions are often limited by mass transfer, which can be greatly improved in continuous-flow chemistry.^[105,106] Reactors for handling solids are nonetheless often significantly more complex and specialized than the ones discussed previously, as solids in microchannels can lead to fouling or clogging.^[103]

In general, three approaches exist to handle gas–solid–liquid reactions: the use of catalyst coatings, packed-bed reactors, and emulsions and suspensions. An overview of the advantages and disadvantages of these approaches is found in Table 2.^[107] These approaches will be discussed in detail in the following sections.

Table 2: Summary of advantages and disadvantages of various flow reactor systems.^[107]

Advantages	Disadvantages
Catalyst coatings	<ul style="list-style-type: none"> • Flexibility in reactor design • High catalyst surface area • Catalytic static mixers can be employed to enhance mass transfer
	<ul style="list-style-type: none"> • Often limited in commercial availability • Reactor material and catalyst are not always compatible with immobilization • Commercial catalytic static mixers are expensive • Challenging or impossible to replace or regenerate deactivated catalyst
Packed-bed reactors	<ul style="list-style-type: none"> • Multiple modes of generation • Compatible with any solid catalyst and solvent • Easy removal of deactivated catalyst • Easy recycling of catalyst • Commercially available
	<ul style="list-style-type: none"> • Columns are expensive and fragile • Limited reactor dimensions • Suboptimal irradiation for photochemistry due to low surface-to-volume ratio • High pressure drop
Emulsions, suspensions, and slurries	<ul style="list-style-type: none"> • Easily assembled from cheap tubing reactors • Efficient mass transfer • Efficient irradiation
	<ul style="list-style-type: none"> • Prone to blockages • Requires very small catalyst particles (usually < 100 nm) • Some catalysts and solvents will be incompatible • Recycling catalyst is more difficult, requires filtration

3.1. Catalyst coatings

One relatively straightforward manner to incorporate solid, heterogeneous catalysts into continuous-flow reactor microchannels is through the application of a thin layer of catalyst coating (1–10 µm) on the inner wall (Figure 9).^[41] Both gas and liquid reactants are then simultaneously introduced into the microchannel, to form a two-phase flow pattern.^[108] These flow patterns are well-defined, which enables the investigation of reaction kinetics and mass transfer.^[109,110] The gas–liquid flow patterns in a catalyst-coated microreactor are similar to the ones described for microchannels without solids, and the most commonly described ones are Taylor (Figure 9A) and annular flow (Figure 9B).^[41] Annular flow is preferred, because the diffusion length through the liquid to the catalyst is short and the thin liquid film allows for a high surface area for the gas to dissolve.^[106,108] This allows for fast heat transfer into the catalyst layer to decrease the formation of hot spots, and fast mass transfer of the liquid phase to the solid catalyst wall.^[41]

The use of wall-coated microchannels is therefore relatively straightforward and easy in its operation. Other multiphasic continuous-flow systems have a much more complex interdependency of the involved parameters, which makes it very difficult to predict and model the performance of the reactor.^[111] Moreover, a large variety of established procedures for the preparation of catalyst coatings has been published.^[41,112] The properties of the catalyst layer inside the microchannels largely influence the performance of the reactor, which has resulted in extensive studies on catalyst supports.^[113]

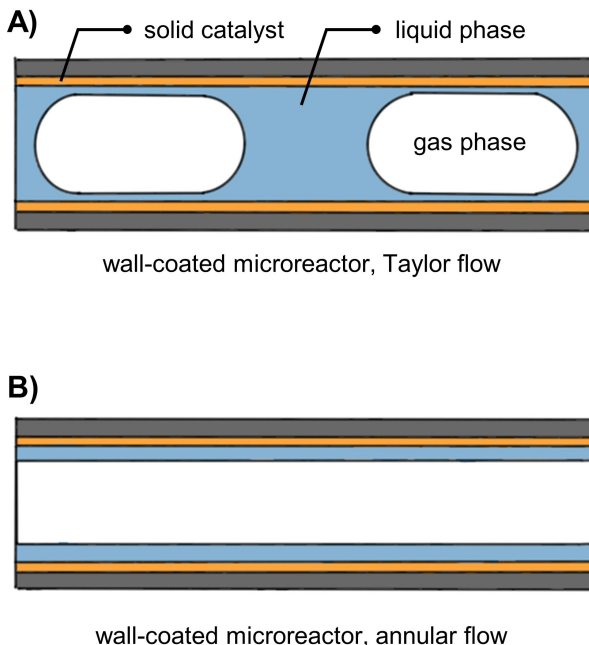
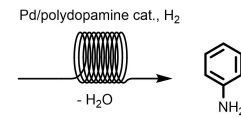


Figure 9. Overview of the two main reactor types for gas-liquid-solid systems in continuous-flow. A) Gas-liquid Taylor flow in a wall-coated microreactor. B) Gas-liquid annular flow in a wall-coated microreactor.^[41]

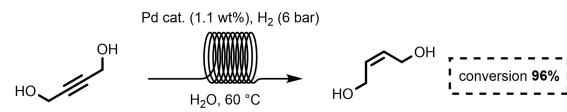
Another advantage is that using these established procedures, well-investigated heterogeneous catalysts can be applied in microreactors. Although this has resulted in various active catalytic flow systems, using well-known noble metal catalysts on solid supports is not without challenges.^[113] For example, Pd nanoparticles on polydopamine supports have shown to be unstable due to their high surface energy, and they easily aggregate to form large particles.^[114] The durability of catalyst layers in microreactors is therefore generally still insufficient.^[113] In 2019, Zhu and co-workers investigated the use of core–shell structured catalysts to prevent the leaching, poisoning, and migration of the active catalyst cores.^[115] However, mass transport of reactants and products to and from the active core would be impaired, resulting in low activity. To circumvent this problem, they investigated the use of porous polydopamine shells for the Pd-catalyzed hydrogenation of nitrobenzene (Scheme 13A).^[116]

As discussed previously, structured microchannels can improve the mass- and heat transfer in continuous-flow systems without increasing the pressure drop, and optimization of microchannel shapes has been investigated.^[63,118] For example, Rehm, Kiwi-Minsker, and co-workers demonstrated this approach using a FFMR containing plates coated with a catalytic layer consisting of Al₂O₃ or ZnO with deposited Pd nanoparticles for the selective hydrogenation of 2-butyne-1,4-diol (Scheme 13B).^[117] Translation of this reaction from batch to continuous-flow mode resulted in a 15-fold increase in performance of the reactor. Recently, Zeng and co-workers investigated a trapezoidal ridge-structured microchannel to improve mixing effects for methanol steam reforming and hydrogen production.^[118] The authors found that compared to an ordinary rectangular microchannel, a ridge-structured microchannel can form a vortex flow, which causes large gas flow disturbances, resulting in improved heat and mass transfer performance (Figure 10). They also observed that with optimized parameters, trapezoidal ridge structured microchannels will have less increasing pressure drop compared to ordinary rectangular microchannels. In another work from 2022, Sun and Sun investigated the effects of four types of structured microchannels (direct, with dimples, sinusoidal, and sinusoidal with dimples) on the performance of steam

A) Hydrogenation of nitrobenzene to aniline, as performed by Zhu and co-workers



B) Hydrogenation of 2-butyne-1,4-diol in the FFMR, as performed by Rehm, Kiwi-Minsker and co-workers



Scheme 13. Various hydrogenations performed in continuous flow. A) Hydrogenation of nitrobenzene.^[115] B) Selective hydrogenation of 2-butyne-1,4-diol.^[117]

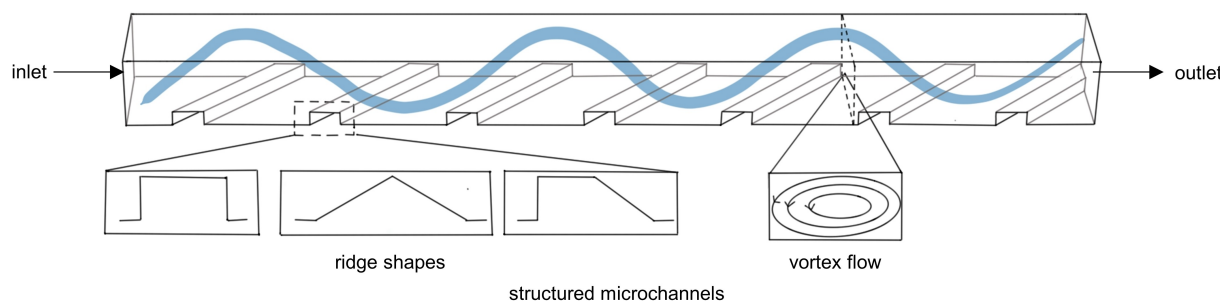


Figure 10. Structured microchannels containing ridge shapes cause large flow disturbances such as vortex flow resulting in improved heat and mass transfer.^[118]

reforming.^[63] The sinusoidal microchannels with dimples were considered the optimal structure of the four types for increased mass- and heat transfer.

3.1.1. Catalytic static mixers

New technologies have been developed in combination with microreactors to further improve mass transfer. Hornung and co-workers developed catalytic static mixers (CSMs), which are specially designed inserts coated with a catalytic layer (Figure 11A).^[119] To demonstrate this concept, they evaluated their CSMs for a series of metal-catalyzed gas-

liquid hydrogenations using vinyl acetate, oleic acid, and cinnamaldehyde (Scheme 14A). The authors asserted that CSMs offer distinct advantages, the utilization of established and easily accessible tubular reactors combined with metal 3D printing technology can generate high value tailored static mixers made of stainless steel able to withstand high temperatures and diverse reaction media.

A subsequent study by the same group showed a scope of hydrogenation reactions of alkenes, alkynes, carbonyls, nitro- and diazo-compounds, nitriles, imines, and halides.^[103] Another advantage of CSMs is that minimal pressure drop is observed in these systems, which implies that scaling up the reactor can be done by increasing the number of CSMs in series or parallel.^[121] Kappe, Williams, and co-workers used this benefit to study the hydrogenation of an API intermediate in systems consisting of 4, 8, or 16 CSMs (Scheme 14B).^[121] They discovered that an increase in the number of CSMs resulted in an increase in the space–time yield, which resulted in a throughput of 174 g h^{-1} for the largest system. According to the authors, scaling up did not promote additional impurity formation, which is a major advantage as the hydrogenation of interest usually forms several troublesome impurities as azo and azoxy intermediates. Another work making use of these scalability benefits was performed by Hornung, Xie, and co-workers on the hydrogenation of flavorings and fragrances using several CSMs inside an intensified tubular reactor.^[122] They observed a space–time yield of $2.66 \text{ kg L}^{-1} \text{ h}^{-1}$ with a high purity (98 %) and full conversion at 24 bar and 130 °C using a novel technique of Pd, Pt, Ru, and Ni supported on alumina and deposited on stainless steel CSMs. Both Pd-Al₂O₃ and Pt-Al₂O₃ CSMs showed high activities and selectivities for C=C and C=O bond reduction. Recently, a novel type of CSM was developed by Kappe, Cantillo, and co-workers for the continuous-flow hydrogenation of nitroaromatics.^[120] The circular cross-section of the CSM was changed to rectangular cross-section channels coated with a layer of Pd/Al₂O₃ as active catalyst (Figure 11B).

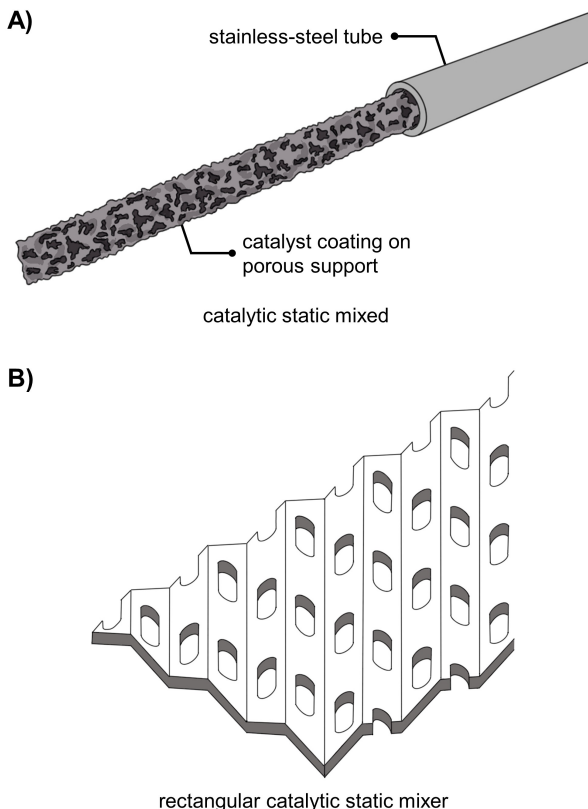
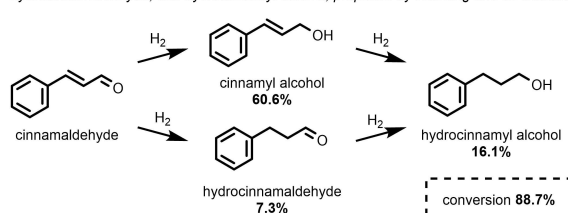


Figure 11. A) Catalytic static mixer inside a stainless-steel tube reactor.^[103] B) Rectangular catalytic static mixer.^[120]

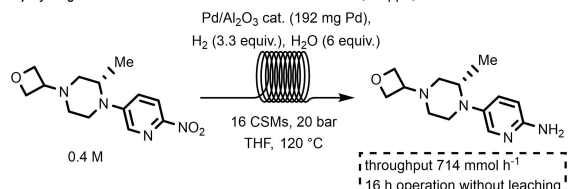
3.1.2. Membrane coating

Another method of utilizing catalytic coatings is in combination with previously discussed tube-in-tube reactors or other

A) Hydrogenation pathway of cinnamaldehyde, yielding cinnamyl alcohol, hydrocinnamaldehyde, and hydrocinnamyl alcohol, proposed by Hornung and co-workers



B) Hydrogenation of API intermediate in continuous flow, Kappe, Williams and co-workers



Scheme 14. A) Hydrogenation of cinnamaldehyde to hydrocinnamyl alcohol using CSMs.^[119] B) Hydrogenation of API intermediate in continuous flow using CSMs.^[121]

membrane reactors. These are particularly interesting because their structure allows for simultaneous generation and separation of products, as well as large contact area between the different phases.^[123] For multiphasic reactions, a gas and liquid stream can contact each other through a semipermeable membrane with a catalyst deposited on its surface. To improve diffusion in such catalytic membrane reactors, Zhu and co-workers demonstrated a compact catalytic hollow fiber membrane reactor for the hydrogenation of nitrobenzene (as previously shown in Scheme 13A).^[123] A Pd nanocatalyst layer was grafted onto the hollow fiber membrane through layer-by-layer self-assembly. The reactor performed well in a 30 h long-term test, although the authors stated that the catalytic ability could be improved. More recently, another system was investigated by Gavriilidis and co-workers that made use of the well-investigated Teflon AF-2400 membrane with adsorbed ex situ synthesized palladium nanoparticles for the hydrogenation of nitrobenzene.^[124] The layer-by-layer assembly of polyelectrolyte multilayers was also used to prevent aggregation of adsorbed nanoparticles, and a variety of differently shaped nanoparticles (spherical, cubical, truncated octahedral, and dendritic) were investigated in terms of conversion and stability. Similarly, for the use of tube-in-tube reactors for gas–liquid systems, an advantage of these setups is an improved control over the gas permeation during the reaction using the Teflon AF-2400 membrane.

3.2. Packed-bed reactors

Although wall-coated microreactors offer numerous advantages in terms of established coating procedures, a disadvantage is that these coating methods can be laborious and energy intensive.^[109] Moreover, in terms of irreversible catalyst deactivation or reactor malfunctioning, catalyst replacement is challenging. In terms of catalyst replacement,

a more convenient way is to keep catalyst particles in place by filters or small inert particles such as glass beads to form a packed-bed reactor (PBR) configuration (Figure 12A).^[41,109] Moreover, the effective catalyst concentration can be significantly higher in PBRs than in batch setups.^[6] Depending on the velocities of the phases, liquid-dominated slug flow (Figure 12B) and gas-continuous flow (Figure 12C) can be observed in PBRs. In 2021, Gavriilidis and co-workers investigated the hydrodynamics and mass transfer properties of these two regimes.^[125]

The use of an inert PBR for enhanced mass transfer in gas–liquid reactions was demonstrated by Fava and co-workers.^[126] This allowed for shorter synthesis routes for pharmaceutically relevant molecules due to the improved safety of oxidation reactions using oxygen gas in continuous flow (Scheme 15). Through their process the production of their key API, namely AZD4635, was safely scaled to 70 g. The original five-step route was exchanged for a three-step synthesis without iridium or palladium, which reduces the use of critical and toxic metals.

According to Kobayashi and co-workers, in 2018 this setup was the most widely used for heterogeneously catalyzed reactions in continuous flow.^[127] This is partly because it allows for the direct use of commercially off-the-shelf or conventionally bulk-synthesized catalysts, which need to be significantly reduced in size compared to macro-scale PBR catalysts ($<50\ \mu m$) to avoid flow maldistribution.^[41,106] Because of this, micro-PBRs are frequently used as platform for rapid screening of catalysts, reaction conditions, and reaction kinetics.^[106] A procedure to characterize and assess the suitability of new heterogeneous catalysts in PBRs for continuous hydrogenations on a pharmaceutical scale has been published by Edwards and co-workers in 2020.^[128] Stahl, Root, and co-workers demonstrated the use of micro-PBRs for admixture screening of multicomponent heterogeneous catalysts for the aerobic oxidative esterification of primary alcohol substrates

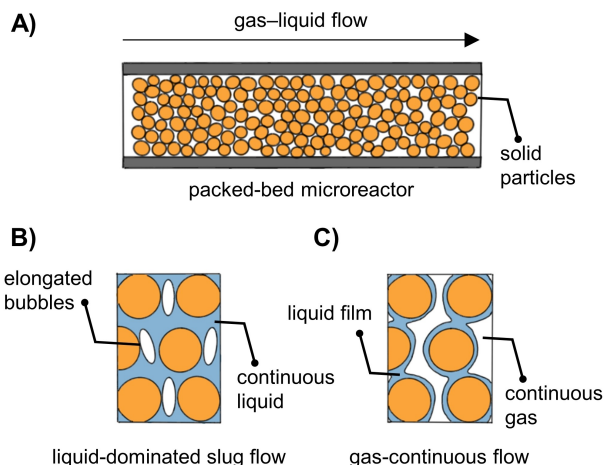
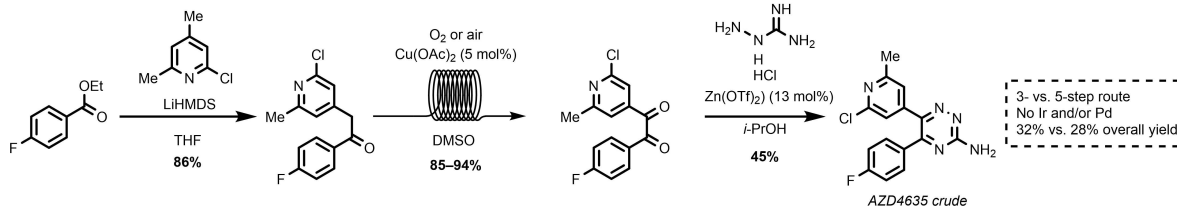


Figure 12. A) Packed-bed microreactor with solid catalyst particles in orange. The two major gas–liquid flow patterns observed over the catalyst bed are B) liquid-dominated slug flow and C) gas-continuous flow.^[41]

Route proposed by Fava and co-workers: subsequent oxidation and condensation reaction



Scheme 15. Newly proposed synthetic route towards API AZD4635.^[126]

(Scheme 16A).^[129] Their approach allowed for the rapid evaluation of over 400 admixture combinations resulting in the discovery of two very effective catalyst compositions. Both of them resulted in >90 % yield, and one of them achieved nearly 60 000 turnovers in a micro-PBR with no apparent loss in catalytic activity.

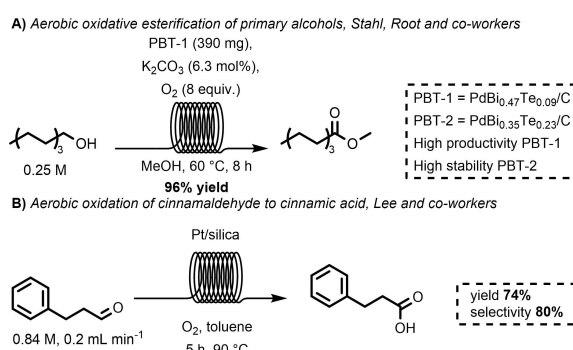
Long-term catalyst stability is a challenge due to poisoning and leaching processes, and several studies investigated the effect of reactor parameters on catalyst deactivation in continuous packed-bed systems, as they allow for relatively fast screening.^[41,131] For example, Gavrilidis and co-workers studied the influence of various parameters in a micro-PBR on the deactivation of a Au–Pd/TiO₂ catalyst used for the oxidation of cinnamyl alcohol.^[132] Deactivation was increased in severity at higher temperatures and higher oxygen gas concentrations, but also differed between substrates.

Similar to other continuous-flow microreactors, micro-PBRs generally have enhanced mass transfer compared to batch processes. Recently, Zhang, Ding, Chen, and co-workers made use of this advantage to increase the catalytic performance of Pd on activated carbon for the hydro-dechlorination of chlorinated organic pollutants.^[133] This reaction is considered to be a safe and effective method for the treatment of pollutants, but suffers from inferior mass transfer performance of batch reactors and often results in catalyst deactivation due to HCl poisoning. Using a micro-PBR, the authors achieved a conversion and selectivity of 100 %, and no apparent deactivation of the catalyst was observed during a 100 h time-on-stream test. Favorable

catalyst stability and mass transfer in micro-PBRs compared to traditional batch systems were also observed by Lee and co-workers in the selective aerobic oxidation of cinnamaldehyde to cinnamic acid using Pt/silica heterogeneous catalysts (Scheme 16B).^[130] Using a micro-PBR, a 37 % increase in net cinnamic acid production was observed after 7 h reaction time compared to batch.

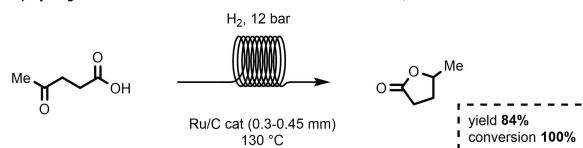
3.2.1. Hydrogenation reactions

One type of reaction that is well-studied in PBRs is hydrogenation, as this reaction often requires high pressures to improve mass transfer of H₂ into the reaction solvent.^[17,134] Also, hydrogenations are exothermic reactions and fine temperature control is key to prevent the formation of hotspots. To investigate the improved mass transfer in a micro-PBR, Yue and co-workers studied the hydrogenation of levulinic acid to γ -valerolactone catalyzed by Ru/C (Scheme 17A).^[109] They achieved complete conversion and obtained an 84 % yield of the corresponding lactone at 130 °C and 12 bar H₂. Under most of the tested operating conditions in the micro-PBR, the reaction proved to be limited by the mass transfer of H₂ through the liquid to the solid phase to the external catalyst surface. The authors suggested that this might be due to relatively large catalyst particles (diameter 0.3–0.45 mm) and due to the relatively low flow rates used. Another recent study by Asano, Miyamura and Kobayashi investigated the mass transfer of

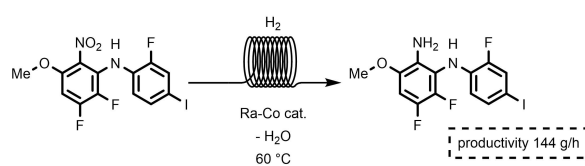


Scheme 16. A) Aerobic oxidative esterification of primary alcohol substrates in continuous flow, shown for 1-octanol.^[129] B) Aerobic oxidation of cinnamaldehyde to cinnamic acid using oxygen gas.^[130]

A) Hydrogenation of levulinic acid over Ru/C in continuous flow, Yue and co-workers.



B) Selective hydrogenation of API intermediate using Ra-Co catalyst, Roggan and co-workers



Scheme 17. A) Hydrogenation of levulinic acid over a Ru/C catalyst in continuous flow.^[109] B) Selective hydrogenation of an API intermediate using a Raney Co catalyst.^[136]

the gas–solid–liquid hydrogenation of toluene in a PBR, using an immobilized Rh–Pt catalyst.^[135] Especially the direct gas–solid contact was found to significantly accelerate the reaction rate.

Raney cobalt and nickel (Ra–Co and Ra–Ni, respectively) are alternatives to the precious metal catalysts in hydrogenation reactions and are less expensive, but can be hazardous to handle. Roggan and co-workers studied the safe use of Ra–Co in a micro-PBR for the selective hydrogenation of a key intermediate for an API on kg per day scale (Scheme 17B).^[136] They found that Ra–Co was a highly selective catalyst at a relatively low temperature of 60°C. Under optimized conditions the product was obtained as a solid that matched the general industrial quality expectations in terms of residual substrate concentrations and side products. To promote implementation of continuous-flow packed-bed reactors for hydrogenation reactions, Lindhardt and co-workers have demonstrated a high mobility reactor unit that can easily be implemented in any Research & Development laboratory.^[137] The authors stated that the reactor is robust and weighs <10 kg. Moreover, usage and setup are fast and simple, allowing for a widely applicable system.

One study in the context of API synthesis was performed by Leitner, Franciò, Poliakoff, and co-workers on the scale-up of a key asymmetric hydrogenation step using a heterogeneous catalyst in a PBR (Scheme 18).^[138] A key step in the formation of the API is the generation of a chiral amine intermediate. Two separate synthesis routes were developed for this step: a transamination of a ketone, and the asymmetric hydrogenation of an enamide. Both batch synthesis routes suffered from challenging product isolation through derivatization of the amine by Boc-protection, which enabled its extraction into an organic phase. The transamination route was preferred, as the hydrogenation required high amounts of catalyst loading under batch conditions. The authors transposed the asymmetric hydrogenation step from batch to flow using a commercially available chiral catalyst (Rh/(S,S)-EthylDuphos), which

would allow for lower catalyst loadings and reduce the environmental footprint of the process.^[138] Their work resulted in excellent catalyst stability at 1 kg scale, resulting in virtually metal-free isolated product (Rh content <1 ppm), with improved purity (>98%) and enantioselectivity (>99%) within 18 h.

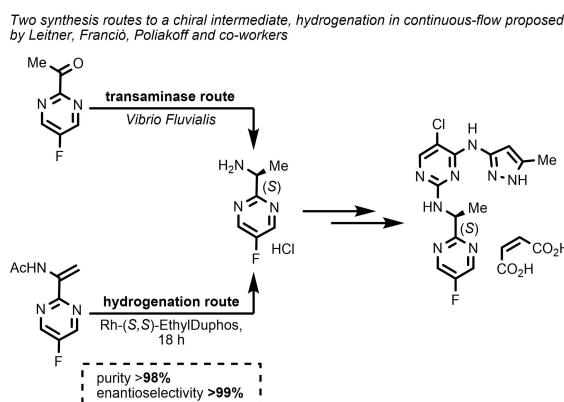
Hydrogenations have also been performed in a telescoped manner. In 2019, Jamison and Russell demonstrated a convergent continuous-flow sequence involving seven chemical transformations to synthesize the antibacterial drug linezolid (Scheme 19A).^[139] The total residence time is 27 min, which is significantly shorter than the reported reaction times for batch procedures (>60 h). The total E-factor of this process is 25, which is relatively low compared to conventional pharmaceutical procedures (25–100). Another work demonstrating the possibilities of performing hydrogenation reactions in a telescoped manner was performed by Andresini, Colella, and co-workers.^[140] The authors demonstrated the chemoselective hydrogenation of 2-azetines using ethyl acetate and cyclopentyl methyl ether as green solvents in continuous flow (Scheme 19B). Moreover, they were able to combine this step with the continuous-flow preparation of the substrates in one protocol.

These hydrogenation reactions can also be telescoped for the synthesis of API intermediates while monitoring the reaction with in-line process analytical technology (PAT). This allows for real-time process control for enhanced safety and product quality.^[142] A prime example of this is a nitration reaction, which can even be performed in a telescoped manner in continuous flow, as demonstrated by Kappe, Williams, and co-workers for the multistep synthesis of the API mesalazine (Scheme 19C).^[141] This route does not only contain a nitration step, but also high temperature hydrolysis and hydrogenation reactions.

Another transformation that benefits from enhanced mass transfer between solids and gases is the formation of C–N bonds through reductive amination.^[143] This important transformation for API synthesis is often performed through substitution reactions with alkyl halides, but this reaction suffers from overreactions and generates a large amount of inorganic salts as waste material. Kobayashi and co-workers studied direct reductive amination of carbonyl compounds using gaseous hydrogen as a more efficient and greener alternative, as only water is generated as byproduct (Scheme 20).^[143] The use of a heterogeneous catalyst in a continuous-flow microreactor was demonstrated to solve several challenges associated with this reaction, such as side reactions, low yields, incompatibility with compounds containing C–C double or triple bonds and other reducible functional groups such as nitro- and cyano-groups.

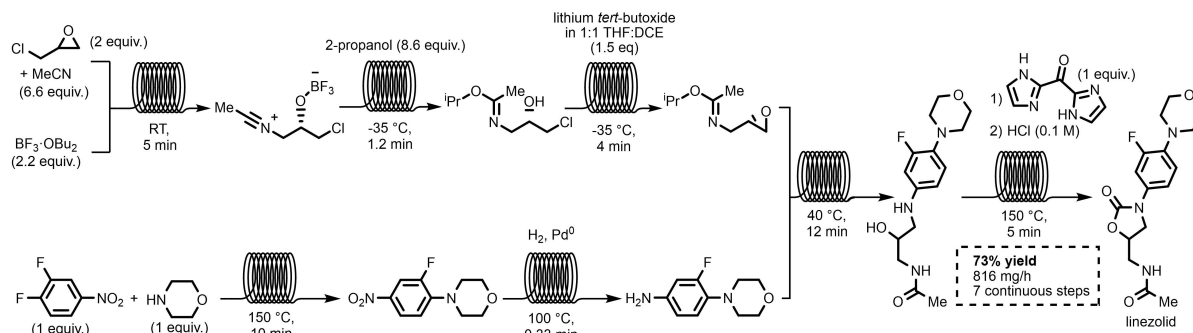
3.2.2. Pressure and flow distribution

Compared to wall-coated microreactors, the use of micro-PBRs usually results in a larger pressure drop. This is due to several factors, such as the use of very fine catalyst particles, less controlled wetting of the catalyst, and more complex

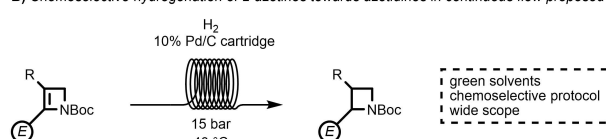


Scheme 18. Two separate synthesis routes for the generation of a chiral intermediate: the transamination of a ketone, and the asymmetric hydrogenation of an enamide. From this intermediate, the hydrogenation was developed further in continuous flow.^[138]

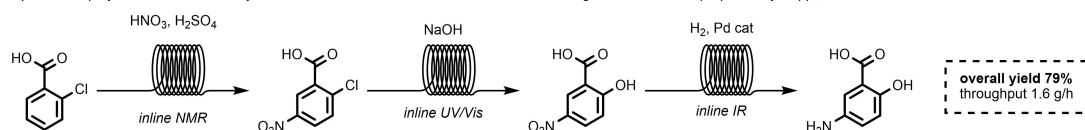
A) Telescoped synthesis of linezolid consisting of 7 steps proposed by Jamison and Russell



B) Chemoselective hydrogenation of 2-azetines towards azetidines in continuous flow proposed by Andresini, Coella, and co-workers

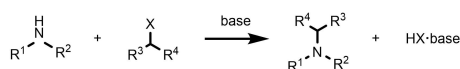


C) Three step synthetic route for the synthesis of mesalazine from 2-chlorobenzoic acid using in-line PAT tools proposed by Kappe, Williams and co-workers

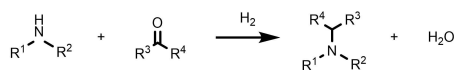


Scheme 19. A) Overview of the telescoped synthetic route towards the API linezolid consisting of seven steps in sequence.^[139] B) Chemoselective hydrogenation of 2-azetines towards azetidines in continuous flow using green solvents.^[140] C) Three-step synthetic route towards the API mesalazine in continuous flow monitored by in-line analysis tools.^[141]

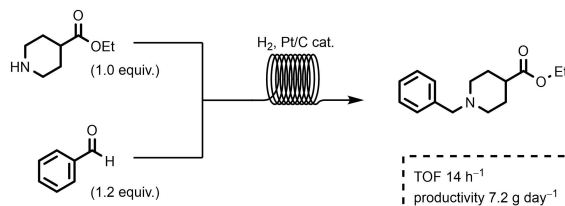
A) Previous route: C–N bond formation through substitution



B) Route proposed by Kobayashi and co-workers:
C–N bond formation through reductive amination



C) Continuous-flow set-up proposed by Kobayashi and co-workers



Scheme 20. C–N bond formation through A) substitution reactions with alkyl halides, and B) reductive amination of carbonyl compounds with hydrogen gas. C) Continuous-flow setup for the reductive amination of carbonyl compounds with hydrogen gas.^[143]

fluid dynamics due to the dominant surface forces over gravitational forces. To optimize the reaction performance, it is important to generate a large interfacial contact area without resulting in a large pressure drop.^[41] In 2021, Zhu and co-workers examined and compared the pressure drop, heat transfer, and conversion of an alkene hydrogenation reaction in a micro-PBR and a microchannel with a catalytic

static mixer.^[144] For both setups 5 wt % Pd/Al₂O₃ was used as catalyst in order to compare the performance of the reactors. The authors demonstrated that catalytic static mixer technology provides several advantages over the frequently used PBRs in terms of lower pressure drop, improved heat transfer, equal or higher turnover frequency and conversion. Zhang, Yan, and co-workers described another strategy to overcome the high pressure drop in micro-PBRs through the direct use of nanosized porous materials.^[145] They suggested the combination of silica spheres (few μm in size) and nanosized materials as the stationary phase, such as a UiO-66-silica composite.

Another challenge of PBRs is the fact that fluid dynamics are relatively uncontrolled compared to other types of microreactors and that unwanted wall flow and channeling inside the column might be observed.^[145] These effects were also described in a comparative study performed by Cherkasov and co-workers on the gas–liquid hydrogenation in powder PBRs compared to catalyst-coated reactors.^[146] They described the reactor performance of the PBR as unrepeatable because the main fluidic path changed continuously due to the mobility of the catalyst powder. Moreover, the residence time distribution was narrower in the wall-coated microreactors, resulting in improved alkene selectivity, whereas over-hydrogenation to alkanes was observed in the PBRs. Lastly, the reaction rate in the catalyst-coated tube reactor was over 5 times higher than in the PBR. The heat transfer was improved compared

to batch processes as it is on a microscale, but not optimal compared to the wall-coated microchannel.^[106]

3.2.3. Structured catalyst supports

To improve the surface area of the catalyst coating inside wall-coated microreactors, porous materials can be employed (e.g., zeolites, metal foam, cloths, fiber, and TiO₂).^[147] An additional advantage of these structured reactors is that they generally have a lower pressure drop than conventional packed-bed reactors. They are therefore promising reactors for gas–solid–liquid reactions in continuous flow.^[148] Moreover, they allow for behavior close to plug flow inside the reaction channels. Extensive literature reports are available on the hydrodynamics of these reactors.^[148–150] Although they have various advantages, structured reactors can suffer from fluid maldistribution and undesired flow regimes.^[148,151]

Monolith reactors are one type of these structured reactors and consist of an interconnected porous solid network that can be formed from organic and/or inorganic polymers.^[106] In 2016, Enke, Tallarek, and co-worker published an extensive review on the use of silica monoliths in microreactors for gas–liquid transformations.^[152] These silica monoliths have proven to be efficient supports for various types of adsorbents and catalysts.^[153]

Metal-based monolith supports are also well-established for efficient catalysis. For example, Zhu and co-workers demonstrated the advantages of the improved catalytic surface area in a monolith reactor containing Pd on a polydopamine modified nickel foam for the hydrogenation of nitrobenzene (reaction previously shown in Scheme 13A).^[147] The conversion of nitrobenzene in the monolith reactor was kept stable at ca. 91 % for over 10 h, whereas the conversion in a similar wall-coated microreactor was kept at 82 % for 3 h, after which it decreased. Another work by Lv, Sun, and co-workers demonstrated the potential of a Cu–Zn/Al foam monolith for the hydrogenation of CO₂ to methanol.^[154] Catalyst-coated metal foams were also employed by Rehm, Kiwi-Minsker, Roggan, and co-workers for the selective hydrogenation of nitrostilbene to form the primary amine without reducing the C=C double bond (Scheme 21).^[155] Two types of catalysts were evaluated using the scale-up strategy.

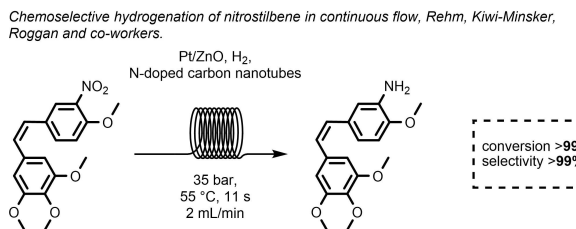
Although it is sometimes complicated to ensure sufficient light penetration in a monolith reactor, it is also

possible to perform photocatalytic reactions in structured microreactors.^[156] For example, Wang and co-workers have performed the photocatalytic degradation of methylene blue using a Ag/AgCl photocatalyst on a polydopamine-modified melamine sponge support to demonstrate its potential for water purification.^[157] Methylene blue was degraded in 10 min under visible light irradiation at 250 L m⁻² h⁻¹. Moreover, the authors demonstrated the recovery of the catalyst, making the monolithic reactor reusable and extending the lifetime of the system. Another work by Leblebici and co-workers demonstrates a setup with a translucent monolith for multiphase photocatalytic reactions.^[158] As a benchmark reaction, they performed the photooxidation of 9,10-diphenylanthracene with singlet oxygen in batch as well as continuous flow (Scheme 22). Their monolith reactor resulted in higher conversions at shorter residence times compared to the batch procedure. Moreover, they demonstrated that this reactor with a translucent monolith could be scaled-up to improve the space-time yield. Gupton and co-workers also investigated high-throughput photooxidations using singlet oxygen in a non-structured immobilized Rose Bengal PBR system instead of using a translucent monolith.^[159]

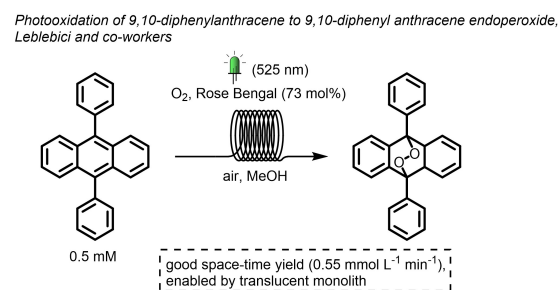
Monoliths are not the only porous catalyst support used inside microchannels. For example, it is also possible to synthesize porous metal fibers that have a three-dimensional structure with interconnected pores. This structure can result in a high porosity and a large specific surface area.^[160] Various types of porous catalyst supports in microchannels were demonstrated for methanol steam reforming reactions.^[160–163]

3.3. Emulsions and suspensions

As stated earlier, handling solids is generally considered to be one of the weaknesses of continuous-flow reactors and batch equipment is often recommended for solid-generating processes. Various strategies have been developed to perform solid-forming reactions in continuous-flow.^[164,165] Although much work has been published on minimizing clogging and fouling, no straightforward solution exists for all equipment or processes.^[166,167] Various clogging mechanisms have been observed in microchannels, such as sieving, bridging, and aggregation of particles (Figure 13). These



Scheme 21. Chemoselective hydrogenation of nitrostilbene to form the primary amine without affecting the C=C double bond in continuous flow.^[155]



Scheme 22. Photooxidation of 9,10-diphenylanthracene with singlet oxygen using Rose Bengal as photosensitizer.^[158]

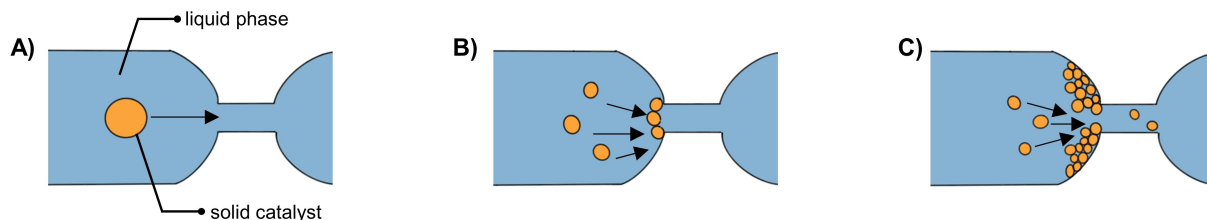


Figure 13. Different clogging mechanisms observed in microchannels: A) sieving, B) bridging, and C) aggregation of particles.^[167]

depend on the relative size of the solid particles compared to the constrictions in the microchannels, as well as the concentration of the suspension, and the interactions between the particles themselves and the particles and the wall.^[167]

3.3.1. Passive mixing

A common strategy for performing heterogeneously catalyzed reactions in continuous flow is through continuous transport of suspended solid catalysts.^[168] Compared to the wall-coated catalyst and the PBR systems, the use of suspended solid nanoparticles in microreactors opens up a new field in heterogeneous catalysis and process intensification. The advantages of heterogeneous and homogeneous catalysis are combined in these systems, such as high activity and selectivity, facile phase separation and reusing or recycling of catalyst, as well as compartmentalization of reactants and products.^[169] Recently, multiple reviews on these systems have been published. In 2022, Pera-Titus and co-workers discussed liquid–liquid and gas–liquid dispersions stabilized by colloidal catalytic particles in continuous-flow systems.^[169] In the same year, Yue and Zong summarized the existing knowledge on the effects of suspended solid particles on the microflow characteristics, such as mass transfer properties.^[168] Moreover, various modelling and experimental studies have been published which investigated the effect on Taylor flow parameters through the introduction of solids in the system.^[170–173]

Several systems have been reported, including colloids (with suspension of nanoparticles), Pickering emulsions

(with nm–μm size solid particles stabilized on two immiscible liquid–liquid interfaces), and slurries (μm-sized particles). Solid particles can be suspended in the continuous (Figure 14A) or dispersed liquid phase (Figure 14B).^[168] Emulsions can be configured with emulsion droplets dispersed in the continuous phase (Figure 14C) or within the dispersed phase (Figure 14D). The dispersed phase can either be gaseous or liquid, but for the scope of this review, only gases are considered. The use of slurries, colloidal solutions, and emulsions allows for flexible production of catalysts and enables high catalyst recovery.^[168] Moreover, it has been reported that more reactive sites are available on the catalyst surface in these systems compared to immobilized photocatalyst systems.^[156]

Systems incorporating suspended solid particles have often demonstrated a good or better heat and/or mass transfer rate than wall-coated catalysts and PBRs.^[168] Moreover, irradiation of the reaction mixture is often improved and more homogeneous, enabling various photochemical reactions requiring a heterogeneous catalyst. Tang, Zhang, and co-workers investigated this improvement for photochemical reactions using gas–liquid–solid Taylor flow for the production of azoxybenzene and azobenzene in a micro-reactor (Scheme 23A).^[174] Graphitic carbon nitride was employed as photocatalyst. The productivity of the system of $26.1 \text{ mmol h}^{-1} \text{ L}^{-1}$ was 5.6 times higher per volume than the batch reactor under the same conditions for the synthesis of azo-compounds. By increasing the inert gas fraction in the system, the total flow rate was increased. This resulted in an increase of the intensity of the recirculation in the slugs, which in turn led to an enhanced local mass transfer. This improvement in efficiency of photochemical reactions

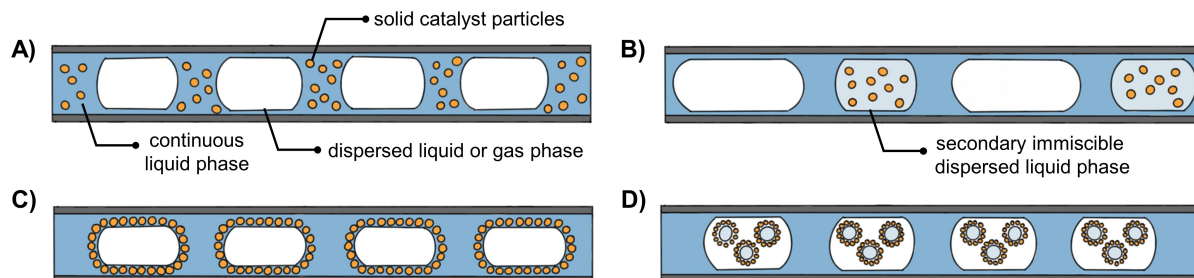
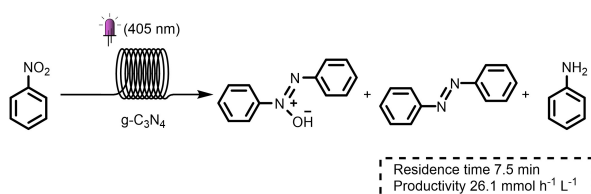
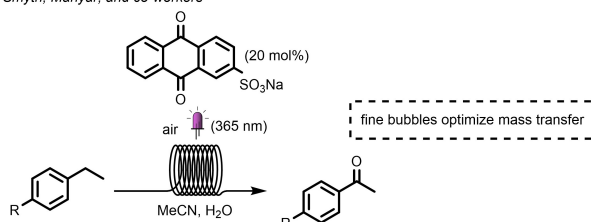


Figure 14. Different types of suspensions and emulsions used in continuous-flow microreactors.^[168] A) Solid catalyst particles suspended in the continuous phase. B) Solid catalyst particles suspended in another (immiscible) dispersed phase. C) Solid catalyst particles in flowing Pickering emulsion with emulsion droplets dispersed in the continuous phase. D) Solid catalyst particles in flowing Pickering emulsion with emulsion droplets dispersed in the dispersed phase.

A) Synthesis of azoxybenzene and azobenzene in a microreactor, Tang, Zhang and co-workers



B) Photooxidation of alkyl benzenes using a sodium anthraquinone sulfate catalyst, Smyth, Manyar, and co-workers

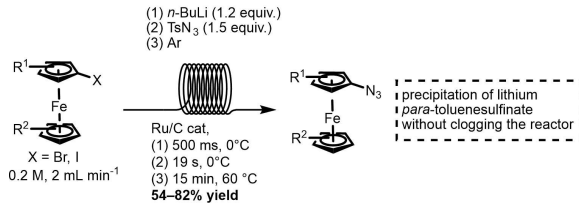


Scheme 23. A) Synthesis of azoxybenzene and azobenzene in a microreactor.^[174] B) Fine bubbles of compressed air enhance gas–liquid mass transfer for photooxidation of alkyl benzenes.^[175]

using suspensions was also demonstrated by Smyth, Manyar, and co-workers who studied the selective photooxidation of alkyl benzenes in a custom-built reactor equipped with a fine bubble generator (Scheme 23B).^[175] The fine bubbles of compressed air enhanced the gas–liquid mass transfer resulting in high conversion of 90 % at short residence times of 5 min.

Solid particles can also be generated during a reaction for which a suspension or emulsion system might be beneficial. An example of this was presented in 2020 by Heretsch, Sarkar, Christmann, and co-workers for the halogen–lithium exchange of ferrocenyl halides and subsequent trapping with tosyl azide to form a variety of functionalized ferrocenyl azides (Scheme 24).^[176] They managed the challenging precipitation of lithium *para*-toluenesulfinate through a triphasic flow regime that prevented blockage of the reactor. The authors stated that this method is general and scalable for the functionalization of ferrocene derivatives in continuous flow and is accelerated to minutes while having an excellent safety and scalability profile.

Synthesis of functionalised ferrocenyl azides in continuous flow, Heretsch, Sarkar, Christmann and co-workers



Scheme 24. A triphasic system employed for the synthesis of ferrocenyl azides in continuous flow.^[176]

3.3.2. Active mixing

One promising technology for the handling of slurries and other solid suspensions is the rotor–stator spinning disk reactor (RS–SDR) (Figure 15). This reactor type uses centrifugal forces in a high shear environment and can significantly improve mass and heat transfer to intensify various chemical reactions through the rotation of a disk in a narrow gap between rotor and stator.^[177,178] The handling of solids in spinning disk reactors has been shown to be possible.^[179] Moreover, RS–SDRs were demonstrated to allow for the scale-up of gas–liquid reactions.^[180] In a recent publication, Noël, Van der Schaaf, and co-workers demonstrated the use of this reactor to handle solid-containing heterogeneous photochemical systems using TiO₂-mediated aerobic photodegradation of methylene blue.^[177] No signs of reactor clogging were observed, moreover the irradiation of the reaction mixture was improved as well as the mass-transfer. Van der Schaaf and co-workers studied the results of micro-mixing in the RS–SDR in the presence of an inert gas.^[178]

An important continuous-flow reactor type able to handle gas–solid–liquid reactions is the continuous stirred-tank reactor (CSTR), which consists of a tank equipped with a stirring system, a feed and withdrawal pipe (Figure 16).^[181] Reactants are continuously fed and the reaction mixture with the products is continuously withdrawn. Although small-scale CSTRs exist, they are often used on a large scale.^[182] They are widely used in the chemical, biological, and petrochemical industries.^[183] The mass transfer characteristics and the mixing in the reactor are key parameters to determine the performance of a CSTR and are therefore investigated for several gas–liquid systems.^[183,184] For example, Atiyeh and co-workers studied the overall volumetric mass transfer coefficient for oxygen gas in a sparged and non-sparged CSTR and found that the mass transfer coefficient increased with an increase in air flow rate as well as increased agitation speed.^[185] They also found that the mass transfer coefficient decreased with an increase in headspace pressure, which the authors attributed to the lower volumetric gas flow rates at high pressure. Increasing

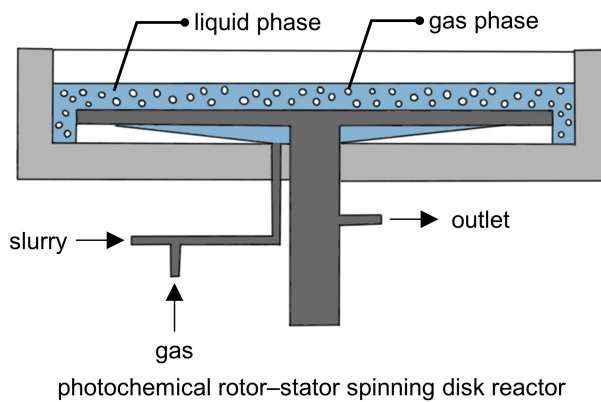


Figure 15. Overview of a photochemical rotor–stator spinning disk technology to handle slurries.^[177]

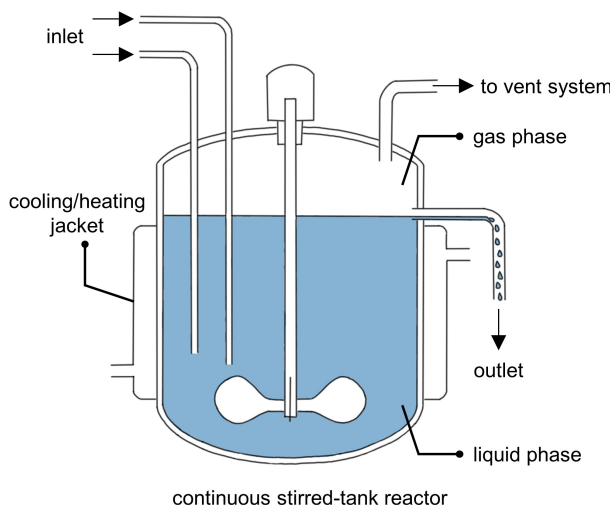
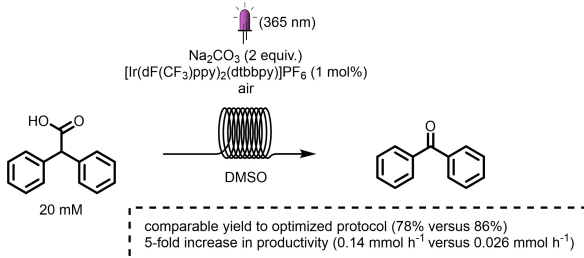


Figure 16. Schematic overview of a continuous stirred-tank reactor.^[187]

the rotational speed seems therefore to be a promising method to prevent the development of unmixed regions. This relation was also studied by Mohammed, Khiadani and Amiraftabi for the performance of a dual helical ribbon impeller.^[186] However, they discovered that increasing the rotational speed above a certain threshold fails to reduce the mixing time but significantly increases power consumption, which led to the conclusion that the rotational speed has an optimum which should be found individually per system. Abdullah and co-worker studied the effect of a different impeller on mixing through comparing the mass transfer coefficients in gas–liquid systems in a CSTR with different types of impellers.^[183]

An advantage of CSTRs is that they can provide long residence times compared to other continuous-flow reactors. Although the residence time distribution in CSTRs is often broad, this can be improved by connecting multiple CSTRs in series to form a cascade.^[182] These cascades are able to effectively handle solids and slurries and are also explored for photochemical approaches.^[188,189] Blacker, Kapur, Marsden, and co-workers proposed a platform based on the CSTR cascade principle for handling gas–solid–liquid reactions and demonstrated its use for a photocatalytic decarboxylative oxidation (Scheme 25).^[190] While keeping the

*A photoredox-catalyzed decarboxylative oxidation of a carboxylic acid,
Blacker, Kapur, Maarsden and co-workers*



Scheme 25. A photocatalytic decarboxylative oxidation of a carboxylic acid.^[190]

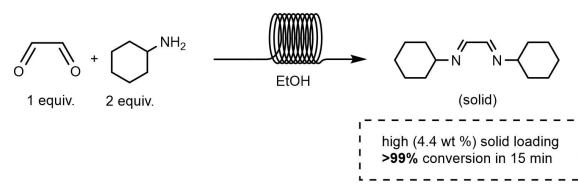
obtained yield comparable to the optimized batch protocol, they were able to achieve a 5-fold increase in productivity.

As mentioned previously, CSTRs are applicable for the handling of solids. Mo and Jensen have designed a miniature CSTR cascade for the handling of solid-generating reactions without clogging.^[191] Two different reactions were performed: the formation of *N,N'*-dicyclohexylethylenediamine from cyclohexylamine and glyoxal (Scheme 26A), and the sulfonylation of 2-octanol with methanesulfonyl chloride (Scheme 26B). Under challenging conditions such as high solid loadings and needle-shaped crystals, an 8 h run was performed without clogging.

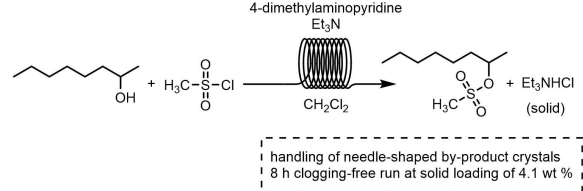
It is also possible to combine CSTRs with other types of reactors. In 2019, Kappe, Dallinger, and co-workers demonstrated the combination of a tube-in-tube reactor and a CSTR, forming a so-called tube-in-CSTR system.^[192] This setup followed from the earlier tube-in-flask setup, which allowed for higher throughput than the tube-in-tube setup for the production of diazoketones, but was a semi-batch setup and therefore could not be safely scaled up with regards to the size of the flask. In this tube-in-flask reactor, the membrane was coiled inside a glass flask to allow the CH₂N₂ gas to diffuse into and be consumed by the substrate solution in the flask. The tube-in-CSTR was therefore developed as a fully continuous version and as proof-of-concept for the three-step synthesis of an α -chloroketone from *N*-protected *L*-phenylalanine and anhydrous CH₂N₂ (Scheme 27). This setup was combined with in-line FTIR to monitor the reaction.

Clogging and mixing issues have also been reduced through implementation of ultrasound in continuous-flow systems.^[193,194] Ultrasound is often used on macroscale to improve mixing, but suffers from non-uniformly generated acoustic fields.^[193] This challenge is solved on the scale of microreactors, as the range of ultrasonic effects are within the scale of the microchannel. When ultrasound and microfluidics are combined correctly, their cumulative performance is often better than the sum of the performances of the

A) Formation of an imine from glyoxal and cyclohexylamine, Mo and Jensen

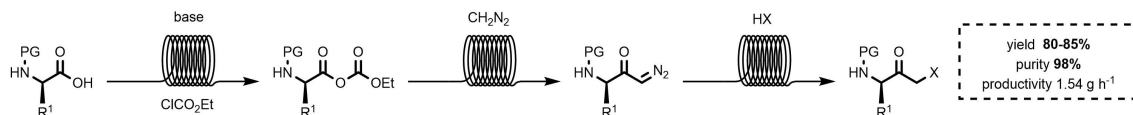


B) Sulfonation of 2-octanol with methanesulfonyl chloride, Mo and Jensen



Scheme 26. Two solid-forming reactions performed in a miniature CSTR cascade: A) the formation of *N,N'*-dicyclohexylethylenediamine from cyclohexylamine and glyoxal, and B) the sulfonylation of 2-octanol with methanesulfonyl chloride.^[191]

Synthesis of α -haloketones from CH_2N_2 and N-protected amino acids, Kappe, Dallinger and co-workers



Scheme 27. Synthesis of α -haloketones from N-protected amino acids and anhydrous CH_2N_2 .^[192]

individual technologies, as they can solve each other's challenges.^[193,195] It is possible to make use of high and low frequency ultrasound, which have different physical effects. The transition regime between high and low frequency ultrasound is generally considered to be between 200 kHz and 1 MHz.^[193]

Chen and co-workers described the residence time distribution and mixing phenomena in ultrasonic microreactors.^[196] Under ultrasonic irradiation, they found that cavitation bubbles were formed in the microreactor, whose motion depends on the bubble size as well as the ultrasound power. According to the authors the cavitation bubbles can act as micromixers, since strong vortices are formed as a result of these bubbles. Interestingly, they describe that the cavitation activity of the bubbles decreases when the channel size is reduced. More work has been published on the mixing effects from ultrasound in microreactors.^[197] A more extensive discussion on these effects can be found in a review published in 2020 by Kuhn and co-workers.^[193] Ultrasound has also been employed for the enhancement of photocatalytic reactions. For example, Noël and co-workers developed an ultrasonic milli-reactor to handle gas–liquid–solid photocatalytic reactions, consisting of a Langevin-type transducer, a sonotrode, and an irradiating cylinder.^[198] The efficacy of the reactor was demonstrated by the photocatalytic aerobic oxidation of benzyl alcohol by TiO_2 particles under UV irradiation (Scheme 28).

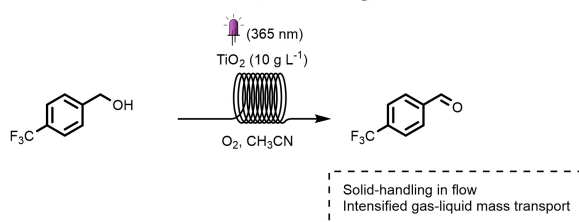
Ultrasonic oscillations can improve mass transfer for multiphasic systems by introducing cavitation and/or surface waves on the gas bubbles, which increases the interfacial surface area.^[195] In 2021, Kuhn and co-workers studied the effect of lower frequency ultrasound (usually around 200 kHz) irradiation on gas–liquid Taylor flow in microchannels.^[195] They found that at lower frequencies, acoustic resonance within liquid slugs could result in confined micro-sprays consisting of large amount of small

liquid droplets. Low-frequency ultrasound could therefore intensify mixing and interfacial mass transfer. Moreover, it can break up agglomerates and detach deposited particles on the inner wall of microchannels to prevent clogging.^[193] High-frequency ultrasound does not result in cavitation effects, but the wavelength in most fluids matches the channel size, making it possible to form a standing wave. This could result in acoustic radiation force, which is useful to displace particles to pressure nodes, and acoustic streaming, which is able to enhance mixing.^[193] It is also possible to combine ultrasound with gas agitation to improve mixing in liquid–liquid systems.^[199] In 2017, Sancheti and Gogate published an extensive overview of reaction types that can be enhanced using ultrasonic reactors.^[200] They state that the use of ultrasonic reactors offers a large potential for sustainable and green chemistry, and suggest that future research focuses on the scale-up of these reactors.

4. Summary and outlook

Continuous-flow technology has enabled transformations that include gaseous reagents, which were deemed either too hazardous or too inefficient under batch conditions. The small scale of microreactors has several intrinsic advantages, such as increased mass and heat transfer, as well as the ability to handle elevated temperatures and pressures to increase solubility of the gases into the solvents. Several reactor setups for the handling of gas–liquid and gas–liquid–solid reactions have been discussed, with each their own advantages and challenges. To optimize the process, it is important to select the right continuous-flow reactor for each specific reaction. Although recent literature discusses improved efficiencies for gas–liquid–solid transformations, the limits of development have not yet been reached. Several knowledge gaps still exist, such as comparative studies on the interfacial area in various flow patterns, as well as comparative studies on the interfacial area in various reactors. Large improvements can still be made in terms of heterogeneous catalyst stability in continuous-flow systems to prevent deactivation and leaching. Also, the use of Pickering emulsions to handle triphasic reactions is still a relatively new research area and could be further explored to improve mass transfer for very fast reactions. We believe that the combination of gases with continuous-flow technologies represents a strong tool to push the chemical industry towards safer and greener processes.

Photocatalytic aerobic oxidation of benzyl alcohol by TiO_2 particles, Noël and co-workers



Scheme 28. Handling of TiO_2 particles for the photocatalytic aerobic oxidation of benzyl alcohol.^[198]

Author Contributions

CRediT: **Annechien A. H. Laporte** formal analysis, investigation, visualisation, writing – original draft, writing – review & editing. **Tom M. Masson** conceptualization, supervision, writing – review & editing. **Stefan D. A. Zondag** writing – review & editing. **Timothy Noël** conceptualization, funding acquisition, supervision.

Acknowledgements

This research was made possible with the generous financial support of the European Union: ERC CoG (FlowHAT, No. 101044355, T.N.) and RIA-NMBP (FlowPhotoChem, No. 862453, T.M.M., S.D.A.Z., and T.N.). The materials presented and views expressed here are the responsibility of the authors only. The EU Commission takes no responsibility for any use made of the provided information.

Conflict of Interest

The authors declare no conflict of interest.

Data Availability Statement

Data sharing is not applicable to this article as no new data were created or analyzed in this study.

Keywords: Flow Chemistry · Gases · Multiphase Reactions · Reactor · Synthetic Methodology

- [1] M. Baumann, T. S. Moody, M. Smyth, S. Wharry, *Org. Process Res. Dev.* **2020**, *24*, 1802–1813.
- [2] J. C. McWilliams, A. D. Allian, S. M. Opalka, S. A. May, M. Journet, T. M. Braden, *Org. Process Res. Dev.* **2018**, *22*, 1143–1166.
- [3] N. Kockmann, P. Thenée, C. Fleischer-Trebes, G. Laudadio, T. Noël, *React. Chem. Eng.* **2017**, *2*, 258–280.
- [4] M. B. Plutschack, B. Pieber, K. Gilmore, P. H. Seeberger, *Chem. Rev.* **2017**, *117*, 11796–11893.
- [5] C. J. Mallia, I. R. Baxendale, *Org. Process Res. Dev.* **2016**, *20*, 327–360.
- [6] M. Guidi, P. H. Seeberger, K. Gilmore, *Chem. Soc. Rev.* **2020**, *49*, 8910–8932.
- [7] D. Dallinger, B. Gutmann, C. O. Kappe, *Acc. Chem. Res.* **2020**, *53*, 1330–1341.
- [8] D. Dallinger, C. O. Kappe, *Curr. Opin. Green Sustain. Chem.* **2017**, *7*, 6–12.
- [9] I. Rossetti, M. Compagnoni, *Chem. Eng. J.* **2016**, *296*, 56–70.
- [10] L. Capaldo, Z. Wen, T. Noël, *Chem. Sci.* **2023**, *14*, 4230–4247.
- [11] L. Wan, M. Jiang, D. Cheng, M. Liu, F. Chen, *React. Chem. Eng.* **2022**, *7*, 490–550.
- [12] R. Gérardy, N. Emmanuel, T. Toupy, V.-E. Kassin, N. N. Tshibalonza, M. Schmitz, J.-C. M. Monbaliu, *Eur. J. Org. Chem.* **2018**, 2301–2351.
- [13] C. A. Hone, A. O’Kearney-McMullan, R. Munday, C. O. Kappe, *ChemCatChem* **2017**, *9*, 3298–3302.
- [14] A. Gavriilidis, A. Constantinou, K. Hellgardt, K. K. Mimi Hii, G. J. Hutchings, G. L. Brett, S. Kuhn, S. P. Marsden, *React. Chem. Eng.* **2016**, *1*, 595–612.
- [15] C. Sambiagio, T. Noël, *Trends Chem.* **2020**, *2*, 92–106.
- [16] D. Cambié, C. Bottecchia, N. J. W. Straathof, V. Hessel, T. Noël, *Chem. Rev.* **2016**, *116*, 10276–10341.
- [17] W. J. Yoo, H. Ishitani, Y. Saito, B. Laroche, S. Kobayashi, *J. Org. Chem.* **2020**, *85*, 5132–5145.
- [18] M. Berton, J. M. de Souza, I. Abdaj, D. T. McQuade, D. R. Snead, *J. Flow Chem.* **2020**, *10*, 73–92.
- [19] A. R. Bogdan, A. W. Dombrowski, *J. Med. Chem.* **2019**, *62*, 6422–6468.
- [20] S. Caille, S. Cui, M. M. Faul, S. M. Mennen, J. S. Tedrow, S. D. Walker, *J. Org. Chem.* **2019**, *84*, 4583–4603.
- [21] R. Porta, M. Benaglia, A. Puglisi, *Org. Process Res. Dev.* **2016**, *20*, 2–25.
- [22] P. Bana, R. Örkényi, K. Lövei, Á. Lakó, G. I. Túró, J. Éles, F. Faigl, I. Greiner, *Bioorg. Med. Chem.* **2017**, *25*, 6180–6189.
- [23] A. Domokos, B. Nagy, B. Szilágyi, G. Marosi, Z. K. Nagy, *Org. Process Res. Dev.* **2021**, *25*, 721–739.
- [24] N. Cherkasov, A. J. Expósito, Y. Bai, E. V. Rebrov, *React. Chem. Eng.* **2019**, *4*, 112–121.
- [25] Z. Dong, Z. Wen, F. Zhao, S. Kuhn, T. Noël, *Chem. Eng. Sci. X* **2021**, *10*, 100097.
- [26] L. Buglioni, F. Raymenants, A. Slattery, S. D. A. Zondag, T. Noël, *Chem. Rev.* **2022**, *122*, 2752–2906.
- [27] S. D. A. Zondag, D. Mazzarella, T. Noël, *Annu. Rev. Chem. Biomol. Eng.* **2023**, *14*, 283–300.
- [28] N. C. Neyt, D. L. Riley, *React. Chem. Eng.* **2021**, *6*, 1295–1326.
- [29] V. Kumar, M. Mridha, A. K. Gupta, K. D. P. Nigam, *Chem. Eng. Sci.* **2007**, *62*, 2386–2396.
- [30] I. V. Gürsel, S. K. Kurt, J. Aalders, Q. Wang, T. Noël, K. D. P. Nigam, N. Kockmann, V. Hessel, *Chem. Eng. J.* **2016**, *283*, 855–868.
- [31] Y. Su, K. Kuijpers, V. Hessel, T. Noël, *React. Chem. Eng.* **2016**, *1*, 73–81.
- [32] K. P. L. L. Kuijpers, M. A. H. H. van Dijk, Q. G. Rumeur, V. Hessel, Y. Su, T. Noël, *React. Chem. Eng.* **2017**, *2*, 109–115.
- [33] A. O. Morgado, J. M. Miranda, J. D. P. Araújo, J. B. L. M. Campos, *Int. J. Multiphase Flow* **2016**, *85*, 348–368.
- [34] S. Haase, *Int. J. Multiphase Flow* **2016**, *87*, 197–211.
- [35] L. Yang, M. J. Nieves-Remacha, K. F. Jensen, *Chem. Eng. Sci.* **2017**, *169*, 106–116.
- [36] N. Erdmann, Y. Su, B. Bosmans, V. Hessel, T. Noël, *Org. Process Res. Dev.* **2016**, *20*, 831–835.
- [37] K. Mandai, T. Yamamoto, H. Mandai, A. Nagaki, *Beilstein J. Org. Chem.* **2022**, *18*, 660–668.
- [38] H. Zhu, Z. Li, X. Yang, G. Zhu, J. Tu, S. Jiang, *Chem. Eng. J.* **2017**, *308*, 606–618.
- [39] S. Haase, S. Marschner, M. M. Ayubi, M. Lange, *Chem. Eng. Process. Process Intensif.* **2022**, *180*, 108687.
- [40] N. Shao, A. Gavriilidis, P. Angeli, *Chem. Eng. Sci.* **2009**, *64*, 2749–2761.
- [41] J. Yue, *Catal. Today* **2018**, *308*, 3–19.
- [42] P. Kumar, A. K. Das, S. K. Mitra, *Phys. Fluids* **2016**, *28*, 072101.
- [43] J. Garcíá-Lacuna, T. Fleiß, R. Munday, K. Leslie, A. O’Kearney-Mcmullan, C. A. Hone, C. O. Kappe, *Org. Process Res. Dev.* **2021**, *25*, 947–959.
- [44] A. Steiner, R. C. Nelson, D. Dallinger, C. O. Kappe, *Org. Process Res. Dev.* **2022**, *26*, 2532–2539.
- [45] M. Movsisyan, E. I. P. Delbeke, J. K. E. T. Berton, C. Battilocchio, V. S. Ley, V. C. Stevens, *Chem. Soc. Rev.* **2016**, *45*, 4892–4928.
- [46] A. Casnati, H. P. L. Gemoets, E. Motti, N. Della Ca’, T. Noël, *Chem. Eur. J.* **2018**, *24*, 14079–14083.

- [47] D. Znidar, D. Dallinger, C. O. Kappe, *ACS Chem. Heal. Saf.* **2022**, *29*, 165–174.
- [48] W. C. Fu, P. M. Macqueen, T. F. Jamison, *Chem. Soc. Rev.* **2021**, *50*, 7378–7394.
- [49] M. Köckinger, C. A. Hone, B. Gutmann, P. Hanselmann, M. Bersier, A. Torvisco, C. O. Kappe, *Org. Process Res. Dev.* **2018**, *22*, 1553–1563.
- [50] M. Vaz, D. Courboin, M. Winter, P. M. C. Roth, *Org. Process Res. Dev.* **2021**, *25*, 1589–1597.
- [51] M. Bernús, D. Mazzarella, J. Stanić, Z. Zhai, A. Yeste-Vázquez, O. Boutureira, A. F. G. Gargano, T. N. Grossmann, T. Noël, *Nat. Synth.* **2023**, <https://doi.org/10.1038/s44160-023-00441-0>.
- [52] G. Laudadio, S. Govaerts, Y. Wang, D. Ravelli, H. F. Koolman, M. Fagnoni, S. W. Djuric, T. Noël, *Angew. Chem. Int. Ed.* **2018**, *57*, 4078–4082.
- [53] S. Leisering, S. Ponath, K. Shakeri, A. Mavroskoufis, M. Kleoff, P. Voßnacker, S. Steinhauer, M. Weber, M. Christmann, *Org. Lett.* **2022**, *24*, 4305–4309.
- [54] S. De Angelis, C. A. Hone, L. Degennaro, P. Celestini, R. Luisi, C. Oliver Kappe, *J. Flow Chem.* **2018**, *8*, 109–116.
- [55] G. Laudadio, Y. Deng, K. van der Wal, D. Ravelli, M. Nuño, M. Fagnoni, D. Guthrie, Y. Sun, T. Noël, *Science* **2020**, *369*, 92–96.
- [56] A. Pulcinella, D. Mazzarella, T. Noël, *Chem. Commun.* **2021**, *57*, 9956–9967.
- [57] S. Bonciolini, T. Noël, L. Capaldo, *Eur. J. Org. Chem.* **2022**, e202200417.
- [58] F. Raymenants, T. M. Masson, J. Sanjosé-Orduna, T. Noël, *Angew. Chem. Int. Ed.* **2023**, *62*, e202308563.
- [59] S. Kim, M. Ishii, R. Kong, G. Wang, *Nucl. Eng. Des.* **2021**, *373*, 111019.
- [60] L. Liu, K. Wang, B. Bai, *Int. J. Multiphase Flow* **2020**, *122*, 103113.
- [61] C. Fernández-Maza, M. Fallanza, L. Gómez-Coma, I. Ortiz, *Chem. Eng. J.* **2022**, *437*, 135192.
- [62] N. Emmanuel, C. Mendoza, M. Winter, C. R. Horn, A. Vizza, L. Dreesen, B. Heinrichs, J.-C. M. Monbaliu, *Org. Process Res. Dev.* **2017**, *21*, 1435–1438.
- [63] W. Lu, R. Zhang, S. Toan, R. Xu, F. Zhou, Z. Z. Sun, Z. Z. Sun, *Chem. Eng. J.* **2022**, *429*, 132286.
- [64] “Corning® Advanced-Flow™ Reactors | Advanced-Flow Reactor Technology | Corning,” can be found under <https://www.corning.com/emea/en/innovation/corning-emerging-innovations/advanced-flow-reactors/achema-2018.html>.
- [65] M. Brzozowski, M. O’Brien, S. V. Ley, A. Polyzos, *Acc. Chem. Res.* **2015**, *48*, 349–362.
- [66] P. Koos, U. Gross, A. Polyzos, M. O’Brien, I. Baxendale, S. V. Ley, *Org. Biomol. Chem.* **2011**, *9*, 6903.
- [67] S. L. Bourne, S. V. Ley, *Adv. Synth. Catal.* **2013**, *355*, 1905–1910.
- [68] S. Newton, S. V. Ley, E. C. Arcé, D. M. Grainger, *Adv. Synth. Catal.* **2012**, *354*, 1805–1812.
- [69] U. Gross, P. Koos, M. O’Brien, A. Polyzos, S. V. Ley, *Eur. J. Org. Chem.* **2014**, *6418*–6430.
- [70] S. Han, M. A. Kashipour, M. Ramezani, M. Abolhasani, *Chem. Commun.* **2020**, *56*, 10593–10606.
- [71] T. Noël, V. Hessel, *ChemSusChem* **2013**, *6*, 405–407.
- [72] M. Ramezani, M. A. Kashipour, M. Abolhasani, *J. Flow Chem.* **2020**, *10*, 93–101.
- [73] B. Musio, E. Gala, S. V. Ley, *ACS Sustainable Chem. Eng.* **2018**, *6*, 1489–1495.
- [74] L. Yang, K. F. Jensen, *Org. Process Res. Dev.* **2013**, *17*, 927–933.
- [75] D. Lokhat, A. K. Domah, K. Padayachee, A. Baboolal, D. Ramjugernath, *Chem. Eng. Sci.* **2016**, *155*, 38–44.
- [76] S. R. L. Gobert, S. Kuhn, L. Braeken, L. C. J. Thomassen, *Org. Process Res. Dev.* **2017**, *21*, 531–542.
- [77] J. Zhang, A. R. Teixeira, H. Zhang, K. F. Jensen, *Anal. Chem.* **2019**, *91*, 4004–4009.
- [78] C. Xue, J. Li, J. P. Lee, P. Zhang, J. Wu, *React. Chem. Eng.* **2019**, *4*, 346–350.
- [79] C. J. Mallia, P. M. Burton, A. M. R. Smith, G. C. Walter, I. R. Baxendale, *Beilstein J. Org. Chem.* **2016**, *12*, 1598–1607.
- [80] H. F. Koolman, S. Kantor, A. R. Bogdan, Y. Wang, J. Y. Pan, S. W. Djuric, *Org. Biomol. Chem.* **2016**, *14*, 6591–6595.
- [81] J. G. H. Hermens, M. L. Lepage, A. Kloekhorst, E. Keller, R. Bloem, M. Meijer, B. L. Feringa, *React. Chem. Eng.* **2022**, *7*, 2280–2284.
- [82] E. C. Aka, E. Wimmer, E. Barré, D. Cortés-Borda, T. Ekou, L. Ekou, M. Rodriguez-Zubiri, F.-X. Felpin, *Org. Process Res. Dev.* **2020**, *24*, 745–751.
- [83] N. Steinfeldt, N. Kockmann, *Ind. Eng. Chem. Res.* **2020**, *59*, 4033–4047.
- [84] Y. Yang, T. Zhang, D. Wang, S. Tang, *J. Taiwan Inst. Chem. Eng.* **2019**, *98*, 27–36.
- [85] J.-M. Commengé, T. Obein, G. Genin, X. Framboisier, S. Rode, V. Schanen, P. Pitiot, M. Matlosz, *Chem. Eng. Sci.* **2006**, *61*, 597–604.
- [86] C. B. McPake, G. Sandford, *Org. Process Res. Dev.* **2012**, *16*, 844–851.
- [87] O. Shvydkiv, K. Jähnisch, N. Steinfeldt, A. Yavorskyy, M. Oelgemöller, *Catal. Today* **2018**, *308*, 102–118.
- [88] T. H. Rehm, S. Gros, P. Löb, A. Renken, *React. Chem. Eng.* **2016**, *1*, 636–648.
- [89] K. H. H. Aziz, *Chemosphere* **2019**, *228*, 377–383.
- [90] J. Chen, F. Xiang, M. Zhu, J. Li, H. Yang, Y. Che, Z. Mao, *ACS Omega* **2021**, *6*, 8394–8402.
- [91] A. A. Mohammed, D. Lokhat, *Rev. Chem. Eng.* **2021**, *37*, 277–303.
- [92] S. J. Pye, S. J. Dalgarno, J. M. Chalker, C. L. Raston, *Green Chem.* **2018**, *20*, 118–124.
- [93] G. Oksdath-Mansilla, R. L. Kucera, J. M. Chalker, C. L. Raston, *Chem. Commun.* **2021**, *57*, 659–662.
- [94] J. Britton, K. A. Stubbs, G. A. Weiss, C. L. Raston, *Chem. Eur. J.* **2017**, *23*, 13270–1327.
- [95] M. Jellicoe, A. Igder, C. Chuah, D. B. Jones, X. Luo, K. A. Stubbs, E. M. Crawley, S. J. Pye, N. Joseph, K. Vimalanathan, Z. Gardner, D. P. Harvey, X. Chen, F. Salvemini, S. He, W. Zhang, J. M. Chalker, J. S. Quinton, Y. Tang, C. L. Raston, *Chem. Sci.* **2022**, *13*, 3375–3385.
- [96] A. Love, D. S. Lee, G. Gennari, R. Jefferson-Loveday, S. J. Pickering, M. Poliakoff, M. George, *Org. Process Res. Dev.* **2021**, *25*, 1619–1627.
- [97] L. Yasmin, X. Chen, K. A. Stubbs, C. L. Raston, *Sci. Rep.* **2013**, *3*, 2282.
- [98] J. G. H. H. Hermens, T. Freese, K. J. Van den Berg, R. Van Gemert, B. L. Feringa, *Sci. Adv.* **2020**, *6*, eabe0026.
- [99] C. A. Clark, D. S. Lee, S. J. Pickering, M. Poliakoff, M. W. George, *Org. Process Res. Dev.* **2018**, *22*, 595–599.
- [100] D. S. Lee, Z. Amara, C. A. Clark, Z. Xu, B. Kakimpa, H. P. Morvan, S. J. Pickering, M. Poliakoff, M. W. George, *Org. Process Res. Dev.* **2017**, *21*, 1042–1050.
- [101] D. S. Lee, M. Sharabi, R. Jefferson-Loveday, S. J. Pickering, M. Poliakoff, M. W. George, *Org. Process Res. Dev.* **2020**, *24*, 201–206.
- [102] D. S. Lee, A. Love, Z. Mansouri, T. H. W. Clarke, D. C. Harrowven, R. Jefferson-Loveday, S. J. Pickering, M. Poliakoff, M. W. George, *Org. Process Res. Dev.* **2022**, *26*, 2674–2684.
- [103] C. H. Hornung, X. Nguyen, A. Carafa, J. Gardiner, A. Urban, D. Fraser, M. D. Horne, D. R. Gunasegaram, J. Tsanaktsidis, *Org. Process Res. Dev.* **2017**, *21*, 1311–1319.

- [104] P. Riente, T. Noël, *Catal. Sci. Technol.* **2019**, *9*, 5186–5232.
- [105] A. J. Exposito, Y. Bai, K. Tchabanenko, E. V. Rebrov, N. Cherkasov, *Ind. Eng. Chem. Res.* **2019**, *58*, 4433–4442.
- [106] A. Tanimu, S. Jaenicke, K. Alhooshani, *Chem. Eng. J.* **2017**, *327*, 792–821.
- [107] C. G. Thomson, A.-L. Lee, F. Vilela, *Beilstein J. Org. Chem.* **2020**, *16*, 1495–1549.
- [108] R. Chen, H. Feng, X. Zhu, Q. Liao, D. Ye, J. Liu, M. Liu, G. Chen, K. Wang, *Chem. Eng. Sci.* **2018**, *175*, 175–184.
- [109] A. Hommes, A. J. Ter Horst, M. Koeslag, H. J. Heeres, J. Yue, *Chem. Eng. J.* **2020**, *399*, 125750.
- [110] Y. Cao, C. Soares, N. Padoin, T. Noël, *Chem. Eng. J.* **2021**, *406*, 126811.
- [111] E. Masson, E. M. Maciejewski, K. M. P. Wheelhouse, L. J. Edwards, *Org. Process Res. Dev.* **2022**, *26*, 2190–2223.
- [112] S. Mehla, J. Das, D. Jampaiah, S. Periasamy, A. Nafady, S. K. Bhargava, *Catal. Sci. Technol.* **2019**, *9*, 3582–3602.
- [113] X. Zhu, H. Feng, R. Chen, Q. Liao, D. Ye, B. Zhang, J. Liu, M. Liu, G. Chen, *RSC Adv.* **2018**, *8*, 5661–5669.
- [114] L. Xu, H. W. Liang, Y. Yang, S. H. Yu, *Chem. Rev.* **2018**, *118*, 3209–3250.
- [115] X. Zhu, H. Feng, R. Chen, Q. Liao, D. Ye, B. Zhang, *Appl. Surf. Sci.* **2019**, *487*, 416–425.
- [116] J. Liu, X. Zhu, Q. Liao, R. Chen, D. Ye, H. Feng, M. Liu, G. Chen, *Chem. Eng. J.* **2018**, *332*, 174–182.
- [117] T. H. Rehm, C. Berguerand, S. Ek, R. Zapf, P. Löb, L. Nikoshvili, L. Kiwi-Minsker, *Chem. Eng. J.* **2016**, *293*, 345–354.
- [118] X. Chu, X. Zeng, T. Zheng, W. Zhuang, Y. Yang, W. Zhou, Y. Hong, *Int. J. Hydrogen Energy* **2020**, *45*, 20859–20874.
- [119] A. Avril, C. H. Hornung, A. Urban, D. Fraser, M. Horne, J. P. Veder, J. Tsanaktsidis, T. Rodopoulos, C. Henry, D. R. Gunasegaram, *React. Chem. Eng.* **2017**, *2*, 180–188.
- [120] R. Lebl, Y. Zhu, D. Ng, C. H. Hornung, D. Cantillo, C. O. Kappe, *Catal. Today* **2022**, *383*, 55–63.
- [121] R. Lebl, S. Bachmann, P. Tosatti, J. Sedelmeier, K. Püntener, J. D. Williams, C. O. Kappe, *Org. Process Res. Dev.* **2021**, *25*, 1988–1995.
- [122] M. Kundra, T. Grall, D. Ng, Z. Xie, C. H. Hornung, *Ind. Eng. Chem. Res.* **2021**, *60*, 1989–2002.
- [123] M. Liu, X. Zhu, R. Chen, Q. Liao, D. Ye, B. Zhang, J. Liu, G. Chen, K. Wang, *Chem. Eng. J.* **2018**, *354*, 35–41.
- [124] B. Venezia, L. Panariello, D. Biri, J. Shin, S. Damilos, A. N. P. Radhakrishnan, C. Blackman, A. Gavriilidis, *Catal. Today* **2021**, *362*, 104–112.
- [125] E. Cao, A. N. P. Radhakrishnan, R. bin Hasanudin, A. Gavriilidis, *Ind. Eng. Chem. Res.* **2021**, *60*, 10489–10501.
- [126] E. Fava, S. Karlsson, M. L. Jones, *Org. Process Res. Dev.* **2022**, *26*, 1048–1053.
- [127] K. Masuda, T. Ichitsuka, N. Koumura, K. Sato, S. Kobayashi, *Tetrahedron* **2018**, *74*, 1705–1730.
- [128] E. Fernandez-Puertas, A. J. Robinson, H. Robinson, S. Sathiyalingam, H. Stubbs, L. J. Edwards, *Org. Process Res. Dev.* **2020**, *24*, 2147–2156.
- [129] D. S. Mannel, M. S. Ahmed, T. W. Root, S. S. Stahl, *J. Am. Chem. Soc.* **2017**, *139*, 1690–1698.
- [130] L. J. Durndell, C. Cucuzzella, C. M. A. Parlett, M. A. Isaacs, K. Wilson, A. F. Lee, *Catal. Today* **2019**, *333*, 161–168.
- [131] E. M. Barreiro, Z. Hao, L. A. Adrio, J. R. van Ommen, K. Hellgardt, K. K. Mimi Hii, *Catal. Today* **2018**, *308*, 64–70.
- [132] G. Wu, G. L. Brett, E. Cao, A. Constantinou, P. Ellis, S. Kuhn, G. J. Hutchings, D. Bethell, A. Gavriilidis, *Catal. Sci. Technol.* **2016**, *6*, 4749–4758.
- [133] Z. Peng, X. Wang, Z. Li, X. Chen, Y. Ding, J. Zhang, *React. Chem. Eng.* **2022**, *7*, 1827–1835.
- [134] H. Miyamura, A. Suzuki, T. Yasukawa, S. Kobayashi, *J. Am. Chem. Soc.* **2018**, *140*, 11325–11334.
- [135] S. Asano, H. Miyamura, M. Matsushita, S. Kudo, S. Kobayashi, J. Hayashi, *J. Flow Chem.* **2023**, <https://doi.org/10.1007/s41981-023-00295-9>.
- [136] M. Ben Said, T. Baramov, T. Herrmann, M. Gottfried, J. Hassfeld, S. Roggan, *Org. Process Res. Dev.* **2017**, *21*, 705–714.
- [137] R. K. Jensen, N. Thykier, M. V. Enevoldsen, A. T. Lindhardt, *Org. Process Res. Dev.* **2017**, *21*, 370–376.
- [138] Z. Amara, M. Poliakoff, R. Duque, D. Geier, G. Franciò, C. M. Gordon, R. E. Meadows, R. Woodward, W. Leitner, *Org. Process Res. Dev.* **2016**, *20*, 1321–1327.
- [139] M. G. Russell, T. F. Jamison, *Angew. Chem.* **2019**, *131*, 7760–7763.
- [140] E. Graziano, D. Cannillo, M. Spennacchio, P. Musci, L. Pisano, M. Andresini, M. Colella, *Tetrahedron Green Chem.* **2023**, *1*, 100003.
- [141] P. Sagmeister, R. Lebl, I. Castillo, J. Rehrl, J. Kruisz, M. Sipek, M. Horn, S. Sacher, D. Cantillo, J. D. Williams, C. O. Kappe, *Angew. Chem. Int. Ed.* **2021**, *60*, 8139–8148.
- [142] M. Rodriguez-Zubiri, F. X. Felpin, *Org. Process Res. Dev.* **2022**, *26*, 1766–1793.
- [143] B. Laroche, H. Ishitani, S. Kobayashi, *Adv. Synth. Catal.* **2018**, *360*, 4699–4704.
- [144] Y. Zhu, B. Bin Mohamad Sultan, X. Nguyen, C. Hornung, *J. Flow Chem.* **2021**, *11*, 515–523.
- [145] J. Zhang, J. Chen, S. S. Peng, S. S. Peng, Z. Zhang, Y. Tong, P. W. Miller, X. P. Yan, *Chem. Soc. Rev.* **2019**, *48*, 2566–2595.
- [146] N. Cherkasov, P. Denissenko, S. Deshmukh, E. V. Rebrov, *Chem. Eng. J.* **2020**, *379*, 122292.
- [147] G. Chen, X. Zhu, R. Chen, Q. Liao, D. Ye, H. Feng, J. Liu, M. Liu, *Chem. Eng. J.* **2018**, *334*, 1897–1904.
- [148] A. Devatine, H. Chaumat, S. Guillaume, B. T. Tchibouanga, F. D. Martínez, C. Julcour, A.-M. M. Billet, *Chem. Eng. Process. Process Intensif.* **2017**, *122*, 277–287.
- [149] Y. Guo, Y. Dong, Z. Lei, W. Ma, *Chem. Eng. Process. Process Intensif.* **2021**, *163*, 108368.
- [150] Y. Guo, C. Dai, Z. Lei, *Chem. Eng. Process. Process Intensif.* **2018**, *125*, 234–245.
- [151] M. Schubert, S. Kost, R. Lange, T. Salmi, S. Haase, U. Hampel, *AICHE J.* **2016**, *62*, 4346–4364.
- [152] D. Enke, R. Gläser, U. Tallarek, *Chem. Ing. Tech.* **2016**, *88*, 1561–1585.
- [153] A. Galarneau, A. Sachse, B. Said, C.-H. Pelisson, P. Boscaro, N. Brun, L. Courtheoux, N. Olivi-Tran, B. Coasne, F. Fajula, *Comptes Rendus Chim.* **2016**, *19*, 231–247.
- [154] Z. Liang, P. Gao, Z. Tang, M. Lv, Y. Sun, *J. CO₂ Util.* **2017**, *21*, 191–199.
- [155] T. H. Rehm, D. Reinhard, H.-J. Kost, C. Hofmann, R. Zapf, P. Löb, Y. Laribi, P. Perrichon, C. Berguerand, L. Kiwi-Minsker, E. Sulman, G. Szribik, H. Richert, J. Lang, M. Gottfried, S. Roggan, *Chem. Eng. J.* **2017**, *316*, 1069–1077.
- [156] D. Heggo, S. Ookawara, *Chem. Eng. Sci.* **2017**, *169*, 67–77.
- [157] J. Duan, X. Fang, C. Li, J. Qu, L. Guo, Y. Zou, M. Xiang, W. Wang, *Colloids Surf. A* **2023**, *659*, 130759.
- [158] M. Jacobs, G. Meir, A. Hakki, L. C. J. Thomassen, S. Kuhn, M. E. Leblebici, *Chem. Eng. Process. Process Intensif.* **2022**, *181*, 109138.
- [159] C. J. Kong, D. Fisher, B. K. Desai, Y. Yang, S. Ahmad, K. Belecki, B. F. Gupton, *Bioorg. Med. Chem.* **2017**, *25*, 6203–6208.
- [160] W. Zhou, Y. Ke, P. Pei, W. Yu, X. Chu, S. Li, K. Yang, *Int. J. Hydrogen Energy* **2018**, *43*, 3643–3654.
- [161] M. M. Sarafraz, M. R. Safaei, M. Goodarzi, M. Arjomandi, *Int. J. Hydrogen Energy* **2019**, *44*, 19628–19639.
- [162] T. Zheng, W. Zhou, D. Geng, Y. Li, Y. Liu, C. Zhang, *Int. J. Hydrogen Energy* **2020**, *45*, 14006–14016.

- [163] T. Zheng, W. Zhou, X. Li, H. You, Y. Yang, W. Yu, C. Zhang, X. Chu, K. S. Hui, W. Ding, *Int. J. Hydrogen Energy* **2020**, *45*, 22437–22447.
- [164] S. K. Kashani, R. J. Sullivan, M. Andersen, S. G. Newman, *Green Chem.* **2018**, *20*, 1748–1753.
- [165] H. Yasukouchi, A. Nishiyama, M. Mitsuda, *Org. Process Res. Dev.* **2018**, *22*, 247–251.
- [166] S. Laue, V. Haverkamp, L. Mleczko, *Org. Process Res. Dev.* **2016**, *20*, 480–486.
- [167] E. Dressaire, A. Sauret, *Soft Matter* **2017**, *13*, 37–48.
- [168] J. Zong, J. Yue, *Ind. Eng. Chem. Res.* **2022**, *61*, 6269–6291.
- [169] D. Dedovets, Q. Li, L. Leclercq, V. Nardello-Rataj, J. Leng, S. Zhao, M. Pera-Titus, *Angew. Chem. Int. Ed.* **2022**, *61*, e202107537.
- [170] L. Ge, Z. Peng, R. Moreno-Atanasio, E. Doroodchi, G. M. Evans, *Ind. Eng. Chem. Res.* **2020**, *59*, 7965–7981.
- [171] Z. Peng, L. Ge, R. Moreno-Atanasio, G. Evans, B. Moghtaderi, E. Doroodchi, *Chem. Eng. J.* **2020**, *396*, 124738.
- [172] Z. Peng, S. Gai, M. Barma, M. M. Rahman, B. Moghtaderi, E. Doroodchi, *Chem. Eng. J.* **2021**, *405*, 126646.
- [173] J. Zong, J. Yue, *Front. Chem. Eng.* **2022**, *3*, 788241.
- [174] Y. Chen, Y. Zhang, H. Zou, M. Li, G. Wang, M. Peng, J. Zhang, Z. Tang, *Chem. Eng. J.* **2021**, *423*, 130226.
- [175] G. Morrison, R. Bannon, S. Wharry, T. S. Moody, N. Mase, M. Hattori, H. Manyar, M. Smyth, *Tetrahedron Lett.* **2022**, *90*, 153613.
- [176] M. Kleoff, J. Schwan, L. Boeser, B. Hartmayer, M. Christmann, B. Sarkar, P. Heretsch, *Org. Lett.* **2020**, *22*, 902–907.
- [177] A. Chaudhuri, S. D. A. Zondag, J. H. A. Schuurmans, J. van der Schaaf, T. Noël, *Org. Process Res. Dev.* **2022**, *26*, 1279–1288.
- [178] A. N. Manzano Martínez, A. Chaudhuri, M. Besten, M. Assirelli, J. van der Schaaf, *Ind. Eng. Chem. Res.* **2021**, *60*, 8677–8686.
- [179] J. Jahanshahi-Anboohi, A. M. Dehkordi, *Ind. Eng. Chem. Res.* **2019**, *58*, 16597–16609.
- [180] A. Chaudhuri, K. P. L. L. Kuijpers, R. B. J. J. Hendrix, P. Shivaprasad, J. A. Hacking, E. A. C. C. Emanuelsson, T. Noël, J. van der Schaaf, *Chem. Eng. J.* **2020**, *400*, 125875.
- [181] P. Trambouze, J. P. Euzen, *Chemical Reactors: From Design to Operation*, Editions Technip, **2004**.
- [182] N. Cherkasov, S. J. Adams, E. G. A. Bainbridge, J. A. M. Thornton, *React. Chem. Eng.* **2023**, *8*, 266–277.
- [183] B. Abdullah, A. A. Adesina, *J. Chem. Technol. Biotechnol.* **2017**, *92*, 2123–2133.
- [184] H. Bashiri, F. Bertrand, J. Chaouki, *Chem. Eng. J.* **2016**, *297*, 277–294.
- [185] K. Liu, J. R. Phillips, X. Sun, S. Mohammad, R. L. Huhnke, H. K. Atiyeh, *Fermentatio* **2019**, *5*, 75.
- [186] M. Amiraftabi, M. Khiadani, H. A. Mohammed, *Chem. Eng. Process. Process Intensif.* **2020**, *148*, 107811.
- [187] “Continuous Stirred Tank Reactor CSTR - UD Technologies,” can be found under <https://udtechnologies.com/continuous-stirred-tank-reactor-cstr/>.
- [188] K. Y. Nandiawale, T. Hart, A. F. Zahrt, A. M. K. Nambiar, P. T. Mahesh, Y. Mo, M. J. Nieves-Remacha, M. D. Johnson, P. García-Losada, C. Mateos, J. A. Rincón, K. F. Jensen, *React. Chem. Eng.* **2022**, *7*, 1315–1327.
- [189] A. Pomberger, Y. Mo, K. Y. Nandiawale, V. L. Schultz, R. Duvadie, R. I. Robinson, E. I. Altinoglu, K. F. Jensen, *Org. Process Res. Dev.* **2019**, *23*, 2699–2706.
- [190] D. Francis, A. J. Blacker, N. Kapur, S. P. Marsden, *Org. Process Res. Dev.* **2022**, *26*, 215–221.
- [191] Y. Mo, K. F. Jensen, *React. Chem. Eng.* **2016**, *1*, 501–507.
- [192] M. Wernik, P. Poechlauer, C. Schmoelzer, D. Dallinger, C. O. Kappe, *Org. Process Res. Dev.* **2019**, *23*, 1359–1368.
- [193] Z. Dong, C. Delacour, K. Mc Caragher, A. P. Udepurkar, S. Kuhn, *Materials* **2020**, *13*, 344.
- [194] G. Chatel, J. C. Colmenares, *Top. Curr. Chem.* **2017**, *375*, 8.
- [195] K. M. Caragher, Z. Dong, D. S. Stephens, M. E. Leblebici, R. Mettin, S. Kuhn, *Ultrason. Sonochem.* **2021**, *75*, 105611.
- [196] Z. Dong, S. Zhao, Y. Zhang, C. Yao, Q. Yuan, G. Chen, *AIChE J.* **2017**, *63*, 1404–1418.
- [197] S. Zhao, C. Yao, Z. Dong, G. Chen, Q. Yuan, *Particuology* **2020**, *48*, 88–99.
- [198] Z. Dong, S. D. A. Zondag, M. Schmid, Z. Wen, T. Noël, *Chem. Eng. J.* **2022**, *428*, 130968.
- [199] S. Zhao, C. Yao, Z. Dong, Y. Liu, G. Chen, Q. Yuan, *Chem. Eng. Sci.* **2018**, *186*, 122–134.
- [200] S. V. Sanchez, P. R. Gogate, *Ultrason. Sonochem.* **2017**, *36*, 527–543.

Manuscript received: October 24, 2023

Accepted manuscript online: December 14, 2023

Version of record online: December 27, 2023